The American Journal of Pathology, Vol. 173, No. 3, September 2008

DOI: 10.2353/ajpath.2008.070902

Musculoskeletal Pathology

Muscle CD31(−) CD45(−) Side Population Cells Promote Muscle Regeneration by Stimulating Proliferation and Migration of Myoblasts

Norio Motohashi,*† Akiyoshi Uezumi,* Erica Yada,* So-ichiro Fukada,* Kazuhiro Fukushima,*¶ Kazuhiko Imaizumi,† Yuko Miyagoe-Suzuki,* and Shin'ichi Takeda*

From the Department of Molecular Therapy, National Institute of Neuroscience, National Center of Neurology and Psychiatry, Tokyo; the Division for Therapies against Intractable Diseases,‡ Institute for Comprehensive Medical Science, Fujita Health University, Aichi; the Department of Immunology,‡ Graduate School of Pharmaceutical Sciences, Osaka University, Osaka; the Laboratory of Physiological Sciences,† Faculty of Human Sciences, Waseda University, Saitama; and the Third Department of Medicine, Neurology, and Rheumatology,¶ Shinshu University School of Medicine, Matsumoto, Japan*

CD31(−) CD45(−) side population (SP) cells are a minor SP subfraction that have mesenchymal stem cell-like properties in uninjured skeletal muscle but that can expand on muscle injury. To clarify the role of these SP cells in muscle regeneration, we injected green fluorescent protein (GFP)-positive myoblasts with or without CD31(−) CD45(−) SP cells into the tibialis anterior muscles of immunodeficient *NOD/scid* mice or dystrophin-deficient *mdx* mice. More GFP-positive fibers were formed after co-transplantation than after transplantation of GFP-positive myoblasts alone in both *mdx* and *NOD/scid* muscles. Moreover, grafted myoblasts were more widely distributed after co-transplantation than after transplantation of myoblasts alone. Immunohistochemistry with anti-phosphorylated histone H3 antibody revealed that CD31(−) CD45(−) SP cells stimulated cell division of co-grafted myoblasts. Genome-wide gene expression analyses showed that these SP cells specifically express a variety of extracellular matrix proteins, membrane proteins, and cytokines. We also found that they express high levels of matrix metalloproteinase-2 mRNA and gelatinase activity. Furthermore, matrix metalloproteinase-2 derived from CD31(−) CD45(−) SP cells promoted migration of myoblasts *in vivo*. Our results suggest that CD31(−) CD45(−) SP cells support muscle regeneration by promoting proliferation and migration of myoblasts. Future studies to further define the molecular and cellular mechanisms of muscle regeneration will aid in the development of cell therapies for muscular dystrophy. ***(Am J Pathol 2008, 173:781–791; DOI: 10.2353/ajpath.2008.070902)***

Regeneration of skeletal muscle is a complex but well-organized process involving activation, proliferation, and differentiation of myogenic precursor cells, infiltration of macrophages to remove necrotic tissues, and remodeling of the extracellular matrix.[1–3] Muscle satellite cells are myogenic precursor cells that are located between the basal lamina and the sarcolemma of myofibers in a quiescent state, and are primarily responsible for muscle fiber regeneration in adult muscle.[4] Recent studies also demonstrated that a fraction of satellite cells self-renew and behave as muscle stem cells *in vivo*.[5,6] On the other hand, several research groups reported multipotent stem cells derived from skeletal muscle. These include muscle-derived stem cells,[7] multipotent adult precursor cells,[8] myogenic-endothelial progenitors,[9] CD34(+) Sca-1(+) cells,[10] CD45(+) Sca-1 (+) cells,[11] mesoangioblasts,[12] and pericytes,[13] and all were demonstrated to contribute to muscle regeneration as myogenic progenitor cells.

Side population (SP) cells are defined as the cell fraction that efficiently effluxes Hoechst 33342 dye and therefore shows a unique pattern on fluorescence-activated cell sorting (FACS) analysis.[14] Muscle SP cells are proposed to be multipotent[15,16] and are clearly distinguished from satellite

Supported by the Ministry of Health, Labor, and Welfare (grant 16b-2 for research on nervous and mental disorders, health science research grant h16-genome-003 for research on the human genome and gene therapy, grants h15-kokoro-021, H18-kokoro-019 for research on brain science); the Ministry of Education, Culture, Sports, Science, and Technology (grants-in-aid for scientific research 16590333 and 18590392); and the Japan Space Forum (ground-based research program for space utilization).

Accepted for publication June 4, 2008.

Supplemental material for this article can be found on *http://ajp.amjpathol.org*.

Address reprint requests to Yuko Miyagoe-Suzuki, M.D., Ph.D., Department of Molecular Therapy, National Institute of Neuroscience, National Center of Neurology and Psychiatry, 4-1-1 Ogawa-higashi, Kodaira, Tokyo 187-8502, Japan. E-mail: miyagoe@ncnp.go.jp.

cells.[17] Previous reports showed that muscle SP cells participated in regeneration of dystrophic myofibers after systemic delivery[15] and gave rise to muscle satellite cells after intramuscular injection into cardiotoxin (CTX)-treated muscle.[17] Muscle SP cells adapted to myogenic characteristics after co-culture with proliferating satellite cells/myoblasts *in vitro*,[17] and expressed a satellite cell-specific transcription factor, Pax7, after intra-arterial transplantation.[18] However, the extent to which muscle SP cells participate in muscle fiber regeneration as myogenic progenitor cells is still primarily unknown. Importantly, Frank and colleagues[19] recently showed that muscle SP cells secret BMP4 and regulate proliferation of BMP receptor1α (+) Myf5^{high} myogenic cells in human fetal skeletal muscle, raising the possibility that SP cells in adult muscle play regulatory roles during muscle regeneration.

Previously we showed that skeletal muscle-derived SP cell fraction are heterogeneous and contain at least three subpopulations: CD31(+) CD45(−) SP cells, CD31(−) CD45(+) SP cells, and CD31(−) CD45(−) SP cells.[20] These three SP subpopulations have distinct origins, gene expression profiles, and differentiation potentials.[20] CD31(+) CD45(−) SP cells account for more than 90% of all SP cells in normal skeletal muscle, take up Ac-LDL, and are associated with the vascular endothelium. CD31(+) CD45(−) SP cells did not proliferate after CTX-induced muscle injury. Bone marrow transplantation experiments demonstrated that CD31(−) CD45(+) SP cells are recruited from bone marrow into injured muscle. A few of them are thought to participate in fiber formation.[21] Cells of the third SP subfraction, CD31(−) CD45(−), constitute only 5 to 6% of all SP cells in adult normal skeletal muscle, but they actively expand in the early stages of muscle regeneration and return to normal levels when muscle regeneration is completed. Although CD31(−) CD45(−) SP cells are the only SP subset that exhibited the capacity to differentiate into myogenic, adipogenic, and osteogenic cells *in vitro*,[20] their myogenic potential *in vivo* is limited compared with satellite cells. Therefore, we hypothesized that CD31(−) CD45(−) SP cells might play critical roles during muscle regeneration other than as myogenic stem cells.

In the present study, we demonstrate that the efficacy of myoblast transfer is markedly improved by co-transplantation of CD31(−) CD45(−) SP cells in both regenerating immunodeficient *NOD/scid* and dystrophin-deficient *mdx* mice. We also show that CD31(−) CD45(−) SP cells increased the proliferation and migration of grafted myoblasts *in vivo* and *in vitro*. We further show that CD31(−) CD45(−) SP cell-derived matrix metalloproteinase (MMP)-2 greatly promotes the migration of myoblasts *in vivo*. Our findings would provide us insights into the molecular and cellular mechanisms of muscle regeneration, and also help us develop cell therapy for muscular dystrophy.

Materials and Methods

Animals

All experimental procedures were approved by the Experimental Animal Care and Use Committee at the National Institute of Neuroscience. Eight- to twelve-week-old C57BL/6 mice and *NOD/scid* mice were purchased from Nihon CLEA (Tokyo, Japan). MMP-2-null mice were obtained from Riken BioResource Center (Tsukuba, Japan).[22] GFP-transgenic mice (GFP-Tg) were kindly provided by Dr. M. Okabe (Osaka University, Osaka, Japan). C57BL/6-background *mdx* mice were generously given by Dr. T. Sasaoka (National Institute for Basic Biology, Aichi, Japan) and maintained in our animal facility.

Isolation of Muscle SP Cells

To evoke muscle regeneration, CTX (10 μmol/L in saline; Sigma, St. Louis, MO) was injected into the tibialis anterior (TA) (50 μl), gastrocnemius (150 μl), and quadriceps femoris muscles (100 μl) of 8- to 12-week-old GFP-Tg mice, C57BL/6 mice, MMP-2-null mice, and their wild-type littermates; 3 days later, SP cells were isolated from the muscles as described by Uezumi and colleagues.[20] In brief, limb muscles were digested with 0.2% type II collagenase (Worthington Biochemical, Lakewood, NJ) for 90 minutes at 37°C. After elimination of erythrocytes by treatment with 0.8% NH_4Cl in Tris-buffer (pH 7.15), mononucleated cells were suspended at 10^6 cells per ml in Dulbecco's modified Eagle's medium (Wako, Richmond, VA) containing 2% fetal bovine serum (JRH Biosciences, Inc., Kansas City, KS), 10 mmol/L Hepes, and 5 μg/ml Hoechst 33342 (Sigma), incubated for 90 minutes at 37°C in the presence or the absence of 50 μmol/L Verapamil (Sigma), and then incubated with phycoerythrin (PE)-conjugated anti-CD31 antibody (1:200, clone 390; Southern Biotechnology, Birmingham, AL) and PE-conjugated anti-CD45 (1:200, clone 30-F11; BD Pharmingen, Franklin Lakes, NJ) for 30 minutes on ice. Dead cells were eliminated by propidium iodide staining. Analysis and cell sorting were performed on an FACS VantageSE flow cytometer (BD Bioscience, Franklin Lakes, NJ). APC-conjugated anti-CD90, Sca-1, CD34, CD49b, CD14, CD124, c-kit, CD14 (BD Pharmingen), CD44 (Southern Biotechnology Associates), and CD133 (eBioscience, San Diego, CA) were used at 1:200 dilution.

Preparation of Satellite Cell-Derived Myoblasts and Macrophages

Satellite cells were isolated from GFP-Tg mice or C57BL/6 mice by using SM/C-2.6 monoclonal antibody[23] and expanded *in vitro* in Dulbecco's modified Eagle's medium containing 20% fetal bovine serum and 2.5 ng/ml of basic fibroblast growth factor (Invitrogen, Carlsbad, CA) for 4 days before transplantation. Macrophages were isolated from C57BL/6 mice 3 days after CTX injection. Mononucleated cells were stained with anti-Mac-1-PE (1:200, clone M1/70; BD PharMingen) and anti-F4/80-APC (1:200, clone CI, A3-1; Serotec, Oxford, UK). Mac-1(+) F4/80(+) cells were isolated by cell sorting as macrophages.

Cell Transplantation

To induce muscle regeneration, 100 μl of 10 μmol/L CTX was injected into the TA muscle of *NOD/scid* muscles,

and 24 hours later, 30 μl of cell suspensions containing 3×10^4 myoblasts, 3×10^4 CD31(−) CD45(−) SP cells, or 3×10^4 GFP(+) myoblasts plus 2×10^4 CD31(−) CD45(−) SP cells were directly injected into the TA muscles of 8-week-old *NOD/scid* or *mdx* mice. At several time points after transplantation, the muscles were dissected, fixed in 4% paraformaldehyde for 30 minutes, immersed in 10% sucrose/phosphate-buffered saline (PBS) and then in 20% sucrose/PBS, and frozen in isopentane cooled with liquid nitrogen.

Retrovirus Transduction in Vitro

Red fluorescent protein (DsRed) cDNA (BD Biosciences, San Diego, CA) was cloned into a retrovirus plasmid, pMXs, kindly provided by Dr. T. Kitamura of the University of Tokyo, Tokyo, Japan.[24] Viral particles were prepared by introducing the resultant pMXs-DsRed into PLAT-E retrovirus packaging cells,[25] and the filtered supernatant was added to the myoblast culture. The next day, DsRed(+) myoblasts were collected by flow cytometry.

Immunohistochemistry

We cut the entire TA muscle tissues on a cryostat into 6-μm cross sections, and observed all serial sections under fluorescence microscopy. We then selected two or three sections in which GFP(+) cells were found most frequently. The sections were then blocked with 5% goat serum (Cedarlane, Hornby, Canada) in PBS for 15 minutes, and then reacted with anti-GFP antibody (Chemicon International, Temecula, CA), anti-laminin α2 antibody (4H8-2; Alexis, San Diego, CA), anti-phospho-histone H3 antibody (Upstate Biotechnology, Lake Placid, NY), or anti-DsRed antibody (Clontech, Palo Alto, CA) at 4°C overnight. Dystrophin was detected using a monoclonal antibody, Dys-2 (Novocastra, Newcastle on Tyne, UK), and a M.O.M. Kit (Vector Laboratories, Burlingame, CA). The sections were then incubated with appropriate combinations of Alexa 488-, 568-, or 594-labeled secondary antibodies (Molecular Probes, Eugene, OR) and TOTO-3 (Molecular Probes), and photographed using a confocal laser-scanning microscope system TCSSP (Leica, Heidelberg, Germany). The area occupied by GFP(+) cells or myofibers was measured by using Image J software (National Institutes of Health, Bethesda, MD) on cross sections from three independent experiments, and defined as the distribution area.

RNA Isolation and Real-Time Polymerase Chain Reaction (PCR)

Total RNA was isolated from muscles using TRIzol (Invitrogen). First strand cDNA was synthesized using a QuantiTect reverse transcription kit (Qiagen, Hilden, Germany). The levels of GFP mRNA and 18S rRNA were quantified using SYBR Premix Ex Taq (Takara, Otsu, Shiga, Japan) on a MyiQ single-color system (Bio-Rad Laboratories, Richmond, CA) following the manufacturer's instructions. Primer sequences for real-time PCR were: 18s rRNA, forward: 5′-TACCCTGGCGGTGGGATTAAC-3′, reverse: 5′-CGAGAGAAGACCACGCCAAC-3′ and EGFP, forward: 5′-GACGTAAACGGCCACAAGTT-3′, reverse: 5′-AAGTCGTGCTGCTTCATGTG-3′. The expression levels of *MMP-2* and *MMP-9* were evaluated by conventional reverse transcriptase (RT)-PCR using the following primers: MMP-2, forward: 5′-TGCAAGGCAGTGGTCATAGCT-3′, reverse: 5′-AGCCAGTCGGATTTGATGCT-3′.

Cell Proliferation Assay

CD31(−) CD45(−) SP cells or 10T1/2 cells were cultured in Dulbecco's modified Eagle's medium containing 20% fetal bovine serum for 5 days, and the supernatants were collected as conditioned medium. Myoblasts were plated on 96-well culture plates at a density of 5000 cells/well and cultured in conditioned medium for 3 days. BrdU was then added to the culture medium (final concentration, 10 μmol/L). Twenty-four hours later, BrdU uptake was quantified by a cell proliferation enzyme-linked immunosorbent assay, a BrdU kit (Roche Diagnostics, Meylan, France), and Lumi-Image F1 (Roche).

Gene Expression Profiling

Total RNAs were extracted from CD31(−) CD45(−) SP cells, macrophages, or myoblasts using an RNeasy RNA isolation kit (Qiagen). cDNA synthesis, biotin-labeled target synthesis, MOE430A GeneChip (Affymetrix, Santa Clara, CA) array hybridization, staining, and scanning were performed according to standard protocols supplied by Affymetrix. The quality of the data presented in this study was controlled by using the Microarray Suite MAS 5.0 (Affymetrix). The MAS-generated raw data were uploaded to GeneSpring software version 7.0 (Silicon Genetics, Redwood City, CA). The software calculates signal intensities, and each signal was normalized to a median of its values in all samples or the 50th percentile of all signals in a specific hybridization experiment. Fold ratios were obtained by comparing normalized data of CD31(−) CD45(−) SP cells and macrophages or myoblasts.

In Situ *Zymography*

CD31(−) CD45(−) SP cells, myoblasts, and macrophages were isolated from regenerating muscles 3 days after CTX injection by cell sorting and collected by a Cytospin3 centrifuge (ThermoShandon, Cheshire, UK) on DQ-gelatin-coated slides (Molecular Probes). The slides were then incubated for 24 hours at 37°C in the presence or absence of GM6001 (a broad-spectrum inhibitor of MMPs, 50 μmol/L; Calbiochem, San Diego, CA) or E-64 (a cysteine protease inhibitor, 50 mmol/L; Calbiochem). Fluorescence of fluorescein isothiocyanate was detected with excitation at 460 to 500 nm and emission at 512 to 542 nm.

Statistics

Statistical differences were determined by Student's unpaired *t*-test. For comparison of more than two groups,

one-way analysis of variance was used. All values are expressed as means ± SE. A probability of less than 5% ($P < 0.05$) or 1% ($P < 0.01$) was considered statistically significant.

Results

Marker Expression on Muscle-Derived CD31(−) CD45(−) SP Cells

When incubated with 5 μg/ml of Hoechst 33342 dye at 37°C for 90 minutes, 1 to 3% of muscle mononuclear cells show the SP phenotype (Figure 1A). Previously, we reported that muscle SP cells can be further divided into three subpopulation, CD31(−) CD45(−) cells, CD31(−) CD45(+) cells, and CD31(+) CD45(−) SP cells (Figure 1B).[20] The CD31(−) CD45(−) SP cells did not express Pax3, Pax7, or Myf5, indicating that they are not yet committed to the muscle lineage.[20] RT-PCR suggested that CD31(−) CD45(−) SP cells have mesenchymal cell characteristics.[20] To further clarify the properties of CD31(−) CD45(−) SP cells, we analyzed their cell surface markers. CD31(−) CD45(−) SP cells were negative for CD124, CD133, CD14, c-kit (Figure 1B), and CD184 (data not shown), weakly positive for CD34 and CD49b, and strongly positive for Sca-1, CD44, and CD90 (Figure 1). The FACS patterns shown in Figure 1B suggested that CD31(−) CD45(−) SP cells are a homogeneous cell population. CD14 is an exception. A small fraction of CD31(−) CD45(−) SP cells were strongly positive for CD14, but the majority weakly expressed this marker. The function of CD14^{high} CD31(−) CD45(−) SP cells remains to be determined.

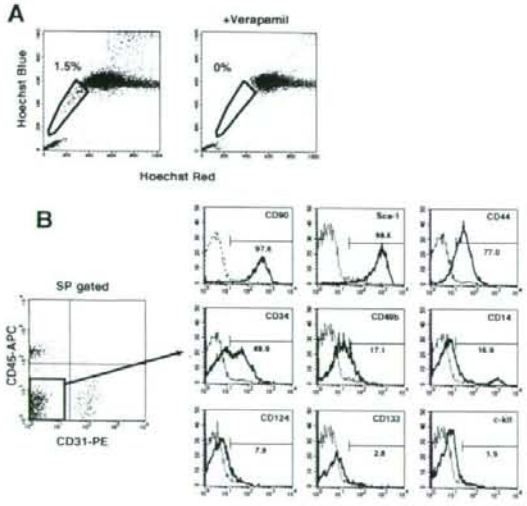

Figure 1. Cell surface markers on CD31(−) CD45(−) SP cells from regenerating muscle. **A:** Mononuclear cells were prepared from limb muscles of C57BL/6 mice at 3 days after CTX injection, incubated with 5 μmol/L Hoechst 33342 with (**right**) or without (**left**) Verapamil, and analyzed by a cell sorter. SP cells are shown by polygons. The numbers indicate the percentage of SP cells in all mononuclear cells. **B: Left:** Expression of CD45 and CD31 on muscle SP cells. **Right:** The expression of surface markers (CD90, Sca-1, CD44, CD34, CD49b, CD14, CD124, CD133, and c-kit) on CD31(−) CD45(−) SP cells was further analyzed by FACS. The *x* axis shows the fluorescence intensity, and the *y* axis indicates cell numbers. Solid lines are with antibodies; dotted lines are negative controls.

Efficiency of Myoblast Transplantation Is Increased by Co-Transplantation of Muscle CD31(−) CD45(−) SP Cells in NOD/scid Mice

To clarify the functions of CD31(−) CD45(−) SP cells during muscle regeneration, we isolated myoblasts from GFP-transgenic mice (GFP-Tg) and injected them (3×10^4 cells/muscle) with or without CD31(−) CD45(−) SP cells (2×10^4 cells/muscle) into TA muscles of immunodeficient *NOD/scid* mice (Figure 2A). CTX was injected into recipient muscles 24 hours before cell transplantation to induce muscle regeneration. Two weeks after transplantation, the contribution of grafted myoblasts to muscle regeneration was investigated by immunodetection of GFP(+) myofibers. Co-transplantation of GFP(+) myoblasts with nonlabeled CD31(−) CD45(−) SP cells produced a higher number of GFP(+) myofibers than transplantation of GFP(+) myoblasts alone (Figure 2, B and C). Furthermore, the average diameter of GFP(+) myofibers was significantly larger in co-transplanted muscles than in muscles transplanted with myoblasts alone (Figure 2D). These results suggest that more myoblasts participated in myofiber formation after co-transplantation than after single transplantation, injected SP cells promoted growth of regenerating myofibers, or both.

Co-transplantation of Myoblasts with Muscle CD31(−) CD45(−) SP Cells Significantly Increased Efficiency of Myoblast Transplantation in mdx Mice

Next, co-transplantation experiments were performed using 8-week-old dystrophin-deficient *mdx* mice as a host. Three kinds of transplantations were performed: 3×10^4 myoblasts derived from GFP-Tg mice, 3×10^4 CD31(−) CD45(−) SP cells derived from GFP-Tg mice, or a mixture of GFP(+) 3×10^4 myoblasts and 2×10^4 CD31(−) CD45(−) SP cells derived from C57BL/6 mice (Figure 3A).

When analyzed at 2 weeks after transplantation, a much higher number of GFP(+) myofibers were detected on cross-sections after co-transplantation of myoblasts and CD31(−) CD45(−) SP cells than after transplantation of GFP(+) myoblasts alone (Figure 3, B and C). On the other hand, transplantation of GFP(+) SP cells alone resulted in formation of few GFP(+) myofibers. This observation is consistent with our previous report.[20] Co-transplantation of myoblasts and CD31(−) CD45(−) SP cells also gave rise to more myofibers expressing dystrophin at the sarcolemma in dystrophin-deficient *mdx* muscles than transplantation of myoblasts alone (data not shown). Again, the diameter of GFP(+) myofibers was significantly larger in co-transplanted muscles than in muscles transplanted with myoblasts or CD31(−) CD45(−) SP cells alone (Figure 3D).

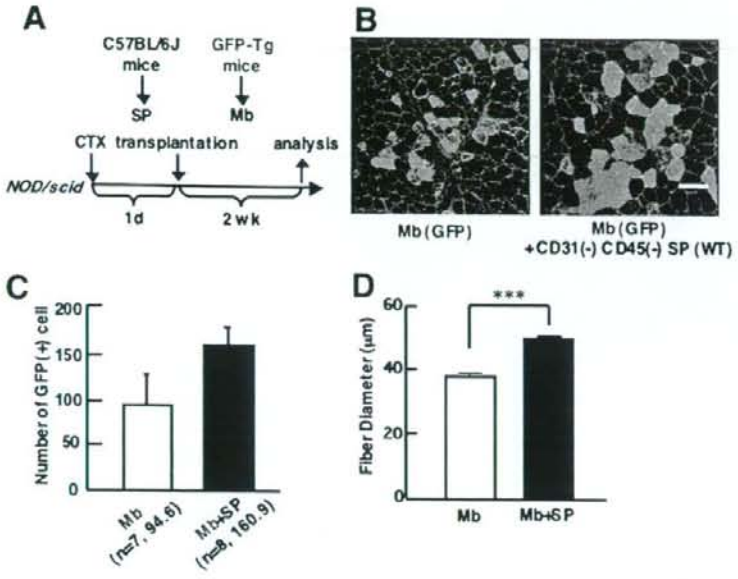

Figure 2. Co-transplantation of myoblasts and CD31(−) CD45(−) SP cells into skeletal muscle of immunodeficient *NOD/scid* mice promotes myofiber formation by transplanted myoblasts. **A:** Schematic protocol of co-transplantation experiments. CTX was injected into TA muscle 1 day before transplantation. Then, GFP(+) myoblasts (Mb) alone or with a mixture of GFP(+) myoblasts and CD31(−) CD45(−) SP cells derived from wild-type (WT) mice were transplanted to CTX-injected TA muscles of 8- to 12-week-old *NOD/scid* mice, and sampled 2 weeks after transplantation. **B:** Cross-sections of transplanted TA muscles stained with anti-GFP (green) and anti-laminin-α2 chain (red) antibodies. Nuclei were stained with TOTO3 (blue). **C:** The number of GFP(+) fibers per cross section of transplanted TA muscle. Values are means with SE (seven to eight mice in each group). $^{**}P < 0.01$. **D:** Average diameters of GFP(+) fibers in the TA muscles transplanted with myoblasts (Mb) or myoblasts plus CD31(−) CD45(−) SP cells (Mb + SP). Values are means with SE. $^{***}P < 0.001$. Scale bar = 80 μm.

The transplantation efficiency of myoblasts in *mdx* mice was 40 to 60% lower than that in *NOD/scid* mice. In the present study, *mdx* mice were not treated with any immunosuppressant. Although cellular infiltration was not evident when examined 2 weeks after transplantation (data not shown), some immune reaction might be evoked and eliminate myoblasts transplanted into *mdx* muscle.

Localization of Transplanted Myoblasts and CD31(−) CD45(−) SP Cells after Intramuscular Injection

To examine the interaction between grafted myoblasts and CD31(−) CD45(−) SP cells during muscle regeneration, we labeled C57BL/6 myoblasts with a retrovirus vector expressing a red fluorescent protein, DsRed. CD31(−) CD45(−) SP cells were isolated from GFP-Tg mice. We then injected a mixture of DsRed(+) myoblasts and GFP(+) CD31(−) CD45(−) SP cells into CTX-injected *NOD/scid* TA muscles. At 24 hours after transplantation, DsRed(+) myoblasts and GFP(+) CD31(−) CD45(−) SP cells were observed clearly (Figure 4A). At 48 hours after transplantation, immunohistochemistry revealed that grafted CD31(−) CD45(−) SP cells expanded, and surrounded both grafted myoblasts and damaged myofibers, but rarely fused with myoblasts (Figure 4B).

CD31(−) CD45(−) SP Cells Promote Proliferation of Myoblasts in Vivo *and* in Vitro

Next, to clarify the mechanism by which co-transplanted CD31(−) CD45(−) SP cells increased the contribution of grafted myoblasts to myofiber regeneration, we investigated the survival of grafted myoblasts after transplantation (Figure 5). GFP(+) myoblasts were injected into TA muscles of *NOD/scid* mice with or without unlabeled CD31(−) CD45(−) SP cells. At 24, 48, and 72 hours after transplantation, injected TA muscles were dissected, and the GFP mRNA level in injected muscles was evaluated by using real-time PCR (Figure 5A). There was a decline of the GFP mRNA level of injected muscles from 24 to 72 hours after injection (Figure 5B) with no differences in survival rates between single transplantation and co-transplantation.

At 48 and 72 hours after transplantation, however, GFP mRNA levels were slightly higher in co-injected muscle than in muscle injected with myoblasts alone (Figure 5B). Therefore, we directly counted the number of GFP(+) myoblasts at 72 hours after transplantation. As shown in Figure 6, A and B, many more GFP(+) myoblasts were detected in co-transplanted muscles than in myoblast-transplanted muscles (Figure 6, A and B). In addition, GFP(+) cells were more widely spread in the co-injected muscles than in muscles transplanted with myoblasts alone (Figure 6C).

To determine whether CD31(−) CD45(−) SP cells promote proliferation of implanted myoblasts, we dissected the muscles at 48 hours after transplantation, and stained the cross-sections with anti-phosphorylated histone H3 antibody, a marker of the mitotic phase of the cell cycle. Co-transplantation of myoblasts with CD31(−) CD45(−) SP cells significantly increased the percentage of mitotic GFP(+) cells compared with transplantation of myoblasts alone (Figure 6D). These observations suggest that co-injection of CD31(−) CD45(−) SP cells promoted proliferation of grafted myoblasts.

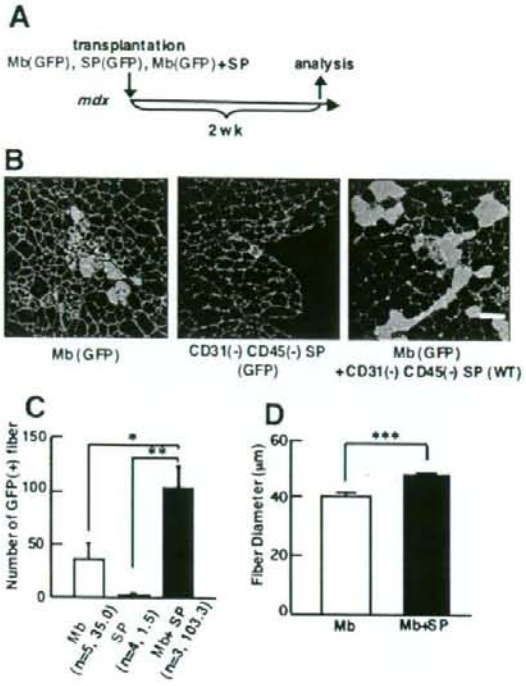

Figure 3. Co-transplantation of CD31(−) CD45(−) SP cells and myoblasts improves efficiency of myoblast transfer in dystrophin-deficient *mdx* mice. **A:** Schematic protocol of experiments. GFP(+) myoblasts alone (3×10^4), GFP(+) CD31(−) CD45(−) SP cells alone (3×10^4 cells), or a mixture of GFP(+) myoblasts (3×10^4) and CD31(−) CD45(−) SP cells (2×10^4) were directly injected into TA muscles of 8-week-old *mdx* mice, and the muscles were sampled 2 weeks after transplantation. **B:** Cross-sections of transplanted TA muscles stained with anti-GFP (green) and anti-laminin-α2 chain (red) antibodies. Nuclei were stained with TOTO3 (blue). **C:** The number of GFP(+) fibers per cross section. Myoblasts gave rise to more myofibers when co-transplanted with CD31(−) CD45(−) SP cells (Mb + SP) than when transplanted alone (Mb). Transplantation of only GFP(+) SP cells resulted in formation of few myofibers (SP). Values are means with SE ($n = 3$ to 5 mice). $^*P < 0.05$, $^{**}P < 0.01$. **D:** Average diameters of GFP(+) fibers in the TA muscles transplanted with myoblasts (Mb) or with myoblasts plus CD31(−) CD45(−) SP cells (Mb + SP). Values are means with SE. $^{***}P < 0.001$. Scale bar = 80 μm.

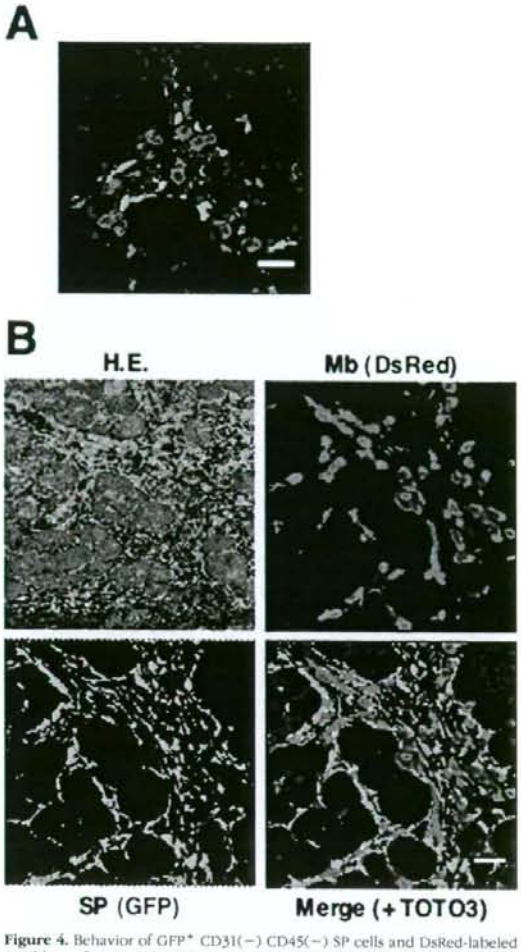

Figure 4. Behavior of GFP$^+$ CD31(−) CD45(−) SP cells and DsRed-labeled myoblasts after transplantation. **A:** *NOD/scid* TA muscles were injected with CTX 24 hours before transplantation. Then, myoblasts transduced with a retrovirus vector expressing DsRed were injected together with GFP(+) CD31(−) CD45(−) SP cells into the muscles. The muscles were dissected 24 hours after the transplantation, sectioned, and stained with anti-DsRed (red) and anti-GFP antibodies (green). Nuclei were stained with TOTO3 (blue). **B:** Representative image of DsRed(+) myoblasts and GFP(+) SP cells 48 hours after co-transplantation. One serial section was stained with H&E. Scale bars = 40 μm.

Next, to examine whether CD31(−) CD45(−) SP cells directly promote proliferation of myoblasts or not, we performed an *in vitro* proliferation assay using primary myoblasts and conditioned medium (CM) of CD31(−) CD45(−) SP cells and CM of 10T1/2 cells. BrdU uptake analysis showed that SP-CM more strongly stimulated the proliferation of myoblasts than 10T1/2-CM did (Figure 6E). The results suggest that CD31(−) CD45(−) SP cells promote proliferation of injected myoblasts at least in part by producing soluble factors.

Gene Expression Profiling of CD31(−) CD45(−) SP Cells

To identify the growth factor produced by CD31(−) CD45(−) SP cells that promotes proliferation of myoblasts, we extracted total RNAs from CD31(−) CD45(−) SP cells, myoblasts, and macrophages isolated from regenerating muscles 3 days after CTX injection, and examined the gene expression in these three cell populations by microarray. Eventually, we identified 192 genes that were expressed at more than 10-fold higher levels in CD31(−) CD45(−) SP cells than in either macrophages or myoblasts. We categorized the 192 genes based on gene ontology, and found that CD31(−) CD45(−) SP cells preferentially express extracellular matrix proteins and cytokines and their receptors (see Supplementary Table S1 at *http://ajp.amjpathol.org*). We found numerous genes involved in wound healing and tissue repair on the gene list, suggesting that CD31(−) CD45(−) SP cells play a regulatory role in the muscle regeneration process. Interestingly, the gene list contained both muscle prolif-

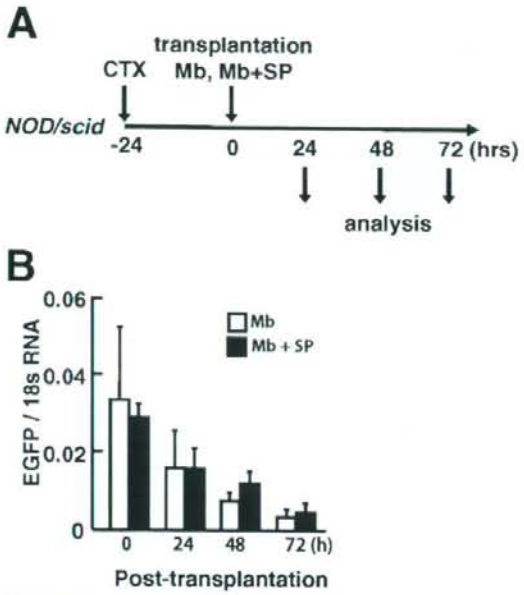

Figure 5. Survival of injected myoblasts in *NOD/scid* mice. **A:** Experimental design. GFP(+) myoblasts alone (3×10^4 cells) or a mixture of GFP(+) myoblasts (3×10^4 cells) and nonlabeled CD31(−) CD45(−) SP cells (2×10^4 cells) were injected into previously CTX-injected TA muscles of *NOD/scid* mice. The muscles were then sampled at 0, 24, 48, and 72 hours after transplantation. **B:** The mRNA level of GFP at each time point was quantified by real-time PCR. The *y* axis shows GFP mRNA levels normalized to 18s RNA with SE ($n = 4$ to 5).

eration or differentiation-promoting (follistatin),[26] and inhibitory factors (eg, insulin-like growth factor binding proteins,[27] Nov[28]). The list also contains regulators of TGF-β (eg, thrombospondins,[29] Prss11,[30] Ltbp3[31]), which would consequently attenuate or stimulate proliferation and differentiation of myoblasts.

CD31(−) CD45(−) SP Cell-Derived MMP-2 Promotes the Migration of Myoblasts

Genome-wide gene expression analysis revealed that CD31(−) CD45(−) SP cells highly express matrix metalloproteinases (see Supplementary Table S1 and Supplementary Figure S1 at *http://ajp.amjpathol.org*). MMPs are a group of zinc-dependent endopeptidases that degrade extracellular matrix components, thereby facilitating cell migration and tissue remodeling.[32,33] Furthermore, MMPs are known to release growth factors stored within the extracellular matrix and process growth factor receptors, resulting in stimulation of cell proliferation.[34–36] Among the MMPs up-regulated in CD31(−) CD45(−) SP cells, we paid special attention to MMP-2 (also called gelatinase A or 72-kDa type IV collagenase). In CTX-injected muscle, MMP-2 activity was shown to be increased concomitantly with the transition from the regeneration phases characterized by the appearance of young myotubes to maturation of the myotubes into multinucleated myofibers[37,38] MMP-2 was also activated in the endomysium of regenerating fibers in dystrophin-deficient muscular dystrophy dogs.[39] Furthermore, MMP-2 transcripts were found in the areas of fiber regeneration, and were localized to mesenchymal fibroblasts in DMD skeletal muscle.[40]

We confirmed that the mRNA level of MMP-2 was much higher in CD31(−) CD45(−) SP cells than in macrophages or myoblasts (Figure 7A). Next, we examined the gelatinolytic activity in CD31(−) CD45(−) SP cells, macrophages, and myoblasts by DQ-gelatin zymography. The cells were directly isolated from regenerating muscle. High gelatinolytic activity was detected in CD31(−) CD45(−) SP cells, compared to myoblasts or macrophages (Figure 7B). Importantly, the signal in MMP-2-null SP cells was considerably weak, compared with wild-type SP cells. The results indicate that DQ-gelatin was degraded mainly (but not exclusively) by MMP-2 in the assay. We hardly detected the green fluorescence in wild-type SP cells in the presence of a broad-spectrum inhibitor of MMPs, GM6001, but not a potent inhibitor of cysteine proteases, E-64, suggesting that other MMPs contribute to gelatin degradation to some extent in the assay. Collectively, these results indicate that CD31(−) CD45(−) SP cells have high MMP-2 activity.

MMP-2 is reported to mediate cell migration and tissue remodeling.[32,33] To directly investigate the effects of MMP-2 on the migration and proliferation of transplanted myoblasts, we injected GFP(+) myoblasts with CD31(−) CD45(−) SP cells prepared from wild-type mice or from MMP-2-null mice into CTX-injected TA muscles of *NOD/scid* mice. There was no difference in the yield of CD31(−) CD45(−) SP cells from regenerating muscle between wild-type and MMP-2-null mice (data not shown). Consistent with this observation, MMP-2-null CD31(−) CD45(−) SP cells proliferated as vigorously as wild-type *in vitro* (data not shown). At 72 hours after transplantation, GFP(+) myoblasts were more widely spread in the muscle co-injected with wild-type CD31(−) CD45(−) SP cells than in the muscles co-injected with MMP-2-deficient CD31(−) CD45(−) SP cells (Figure 7C). In contrast, there was no difference in the number of GFP(+) myoblasts between two groups (Figure 7D). These results strongly suggest that MMP-2 derived from CD31(−) CD45(−) SP cells significantly promotes migration of myoblasts, but does not influence the proliferation of myoblasts.

Discussion

We previously reported a novel SP subset: CD31(−) CD45(−) SP cells.[20] They are resident in skeletal muscle and are activated and vigorously proliferate during muscle regeneration. RT-PCR analysis suggested that CD31(−) CD45(−) SP cells are of mesenchymal lineage, and indeed they differentiated into adipocytes, osteogenic cells, and muscle cells after specific induction *in vitro*.[20] In the present study, we further characterized CD31(−) CD45(−) SP cells and found that co-transplantation of CD31(−) CD45(−) SP cells markedly improves the efficacy of myoblast transfer to dystrophic *mdx* mice. Our

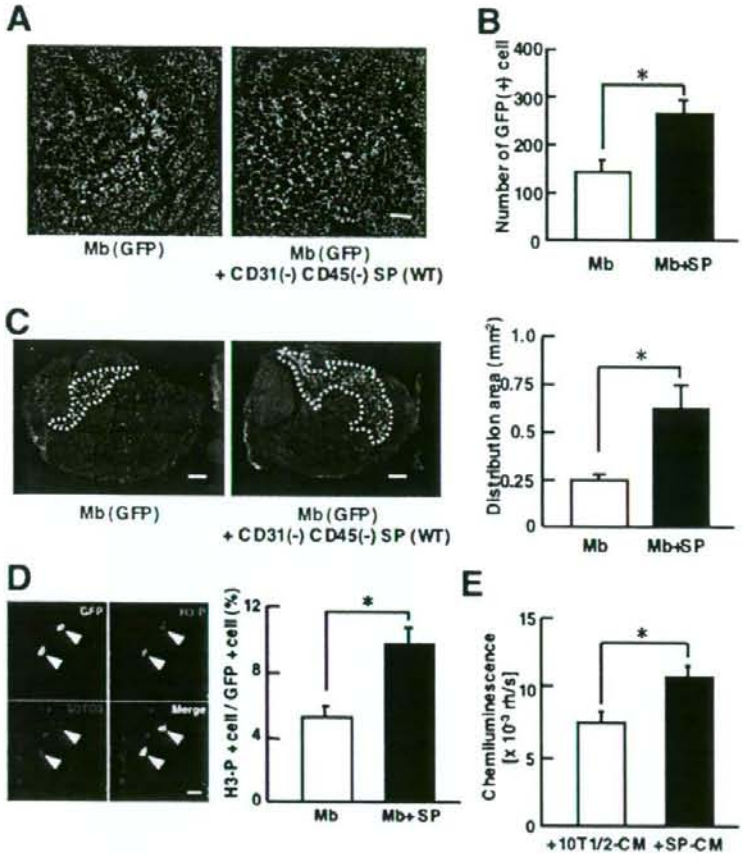

Figure 6. CD31(−) CD45(−) SP cells promote proliferation of myoblasts *in vitro* and *in vivo*. **A:** Representative images of cross sections of 72-hour samples stained with anti-GFP (green) and anti-laminin-α2 chain (red) antibodies. GFP(+) myoblasts are more widely scattered in injected muscle when co-transplanted with CD31(−) CD45(−) SP cells, compared with single transplantation. **B:** The number of GFP(+) cells per cross section of TA muscles injected with myoblasts or myoblasts and CD31(−) CD45(−) SP cells. Values were means with SE (n = 4 to 5). *$P < 0.05$. **C: Left:** Representative distributions of GFP(+) myoblasts/myotubes 72 hours after transplantation. **Right:** Distribution area (marked by white dotted lines in **left** panels) was measured by Image J software. Values were means with SE (n = 4 to 5). *$P < 0.05$. **D:** GFP(+) myoblasts were transplanted into CTX-injected TA muscles of *NOD/scid* mice with (Mb + SP) or without CD31(−) CD45(−) SP cells (Mb). Forty-eight hours after transplantation, the muscles were dissected, sectioned, and stained with anti-phosphorylated histone-H3 (H3-P) (red) and anti-GFP (green) antibodies. **Arrowheads** indicate H3-P(+) GFP(+) cells. The **right** graph shows the percentage of H3-P(+) GFP(+) myoblasts in single-transplanted muscle (Mb) or in co-transplanted muscle (Mb + SP). The values are means with SE (n = 3). *$P < 0.05$. **E:** Myoblasts were cultured for 3 days in conditioned medium of either CD31(−) CD45(−) SP cells (SP-CM) or 10T1/2 cells (10T1/2-CM) and then cultured for an additional 24 hours in the presence of BrdU. The vertical axis shows BrdU uptake by myoblasts. Values are means with SE (n = 6). *$P < 0.05$. Scale bars: 100 μm (**A**); 200 μm (**C**); 80 μm (**D**).

findings suggest that endogenous CD31(−) CD45(−) SP cells support muscle regeneration by stimulating proliferation and migration of myoblasts.

Are CD31(−) CD45(−) SP Cells Mesenchymal Stem Cells?

Analysis of cell surface antigens on CD31(−) CD45(−) SP cells suggests that they are a homogeneous population. Several reports showed that mesenchymal stem cells (MSCs) express CD44, CD90, but not CD31, CD45, or CD14.[41,42] The expression patterns of these markers on CD31(−) CD45(−) SP cells and their differentiation potentials into osteogenic cells, adipocytes, and myogenic cells suggest that CD31(−) CD45(−) SP cells are closely related to MSCs.[20] On the other hand, the expression of PDGFRβ,[20] CD44, CD49b, CD90, and the lack of CD133 expression on CD31(−) CD45(−) SP cells are similar to those of human pericytes.[13] Unlike human pericytes, however, CD31(−) CD45(−) SP cells have limited myogenic potential *in vivo*.[13,20] The relationship between CD31(−) CD45(−) SP cells and MSCs or pericytes remains to be determined in a future study.

CD31(−) CD45(−) SP Cells Promote Proliferation of Myogenic Cells

In the present study, we demonstrated that the efficiency of myoblast transfer is greatly improved by co-transplantation of CD31(−) CD45(−) SP cells. Transplanted CD31(−) CD45(−) SP cells proliferated in the injection site and surrounded both engrafted myoblasts and damaged myofibers, but rarely fused with myoblasts (Figure 4). Transplantation of CD31(−) CD45(−) SP cells alone contributed little to myofiber formation. Therefore, the improvement in efficiency of myoblast transfer by co-transplantation is not attributable to differentiation of CD31(−) CD45(−) SP cells into muscle fibers.

Because the conditioned medium from CD31(−) CD45(−) SP cells modestly stimulated the proliferation of myoblasts *in vitro*, when compared with CM of 10T1/2 cells, it is possible that CD31(−) CD45(−) SP cells stimulated proliferation of myoblasts by secreting growth factors. CD31(−) CD45(−) SP cells are found in close vicinity to myoblasts 48 hours after transplantation. Therefore, even low levels of growth factors produced by CD31(−) CD45(−) SP cells may effectively stimulate the prolifera-

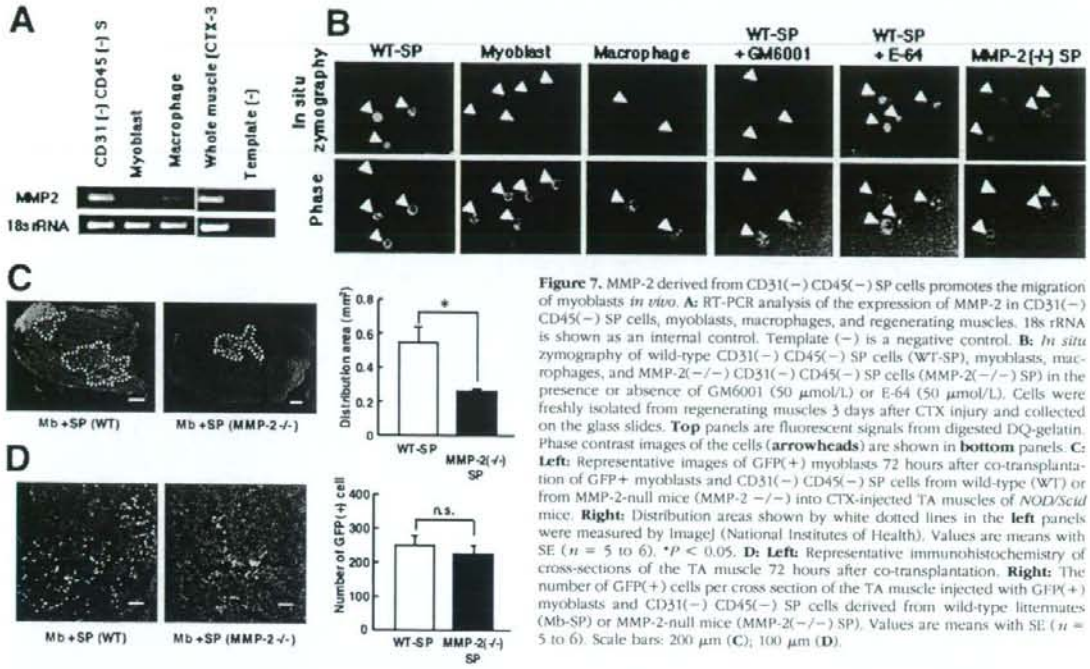

Figure 7. MMP-2 derived from CD31(−) CD45(−) SP cells promotes the migration of myoblasts *in vivo*. **A:** RT-PCR analysis of the expression of MMP-2 in CD31(−) CD45(−) SP cells, myoblasts, macrophages, and regenerating muscles. 18s rRNA is shown as an internal control. Template (−) is a negative control. **B:** *In situ* zymography of wild-type CD31(−) CD45(−) SP cells (WT-SP), myoblasts, macrophages, and MMP-2(−/−) CD31(−) CD45(−) SP cells (MMP-2(−/−) SP) in the presence or absence of GM6001 (50 μmol/L) or E-64 (50 μmol/L). Cells were freshly isolated from regenerating muscles 3 days after CTX injury and collected on the glass slides. **Top** panels are fluorescent signals from digested DQ-gelatin. Phase contrast images of the cells (**arrowheads**) are shown in **bottom** panels. **C: Left:** Representative images of GFP(+) myoblasts 72 hours after co-transplantation of GFP+ myoblasts and CD31(−) CD45(−) SP cells from wild-type (WT) or from MMP-2-null mice (MMP-2 −/−) into CTX-injected TA muscles of *NOD/Scid* mice. **Right:** Distribution areas shown by white dotted lines in the **left** panels were measured by ImageJ (National Institutes of Health). Values are means with SE (n = 5 to 6). *$P < 0.05$. **D: Left:** Representative immunohistochemistry of cross-sections of the TA muscle 72 hours after co-transplantation. **Right:** The number of GFP(+) cells per cross section of the TA muscle injected with GFP(+) myoblasts and CD31(−) CD45(−) SP cells derived from wild-type littermates (Mb-SP) or MMP-2-null mice (MMP-2(−/−) SP). Values are means with SE (n = 5 to 6). Scale bars: 200 μm (**C**); 100 μm (**D**).

tion of myoblasts. Importantly, several reports showed that MSCs secrete a variety of cytokines and growth factors, which suppress the local immune system, inhibit fibrosis and apoptosis, enhance angiogenesis, and stimulate mitosis and differentiation of tissue-specific stem cells.[43] On the gene list, we found a variety of cytokines/chemokines and their regulators (see Supplementary Table S1 at *http://ajp.amjpathol.org*). These molecules may directly or indirectly stimulate proliferation of myoblasts.

MMP-2 Derived from CD31(−) CD45(−) SP Cells Promotes the Migration of Myoblasts

Transplanted GFP(+) myoblasts were more widely spread in injected muscle when co-injected with CD31(−) CD45(−) SP cells than when transplanted alone (Figure 6C). MMP-2 is a candidate molecule that promotes migration of myoblasts. MMP-2 plays a critical role in myogenesis[44] and is up-regulated in muscle regeneration (see Supplementary Figure S2 at *http://ajp.amjpathol.org*).[38] MMP-2 expression is also detected in regenerating areas of dystrophic muscles.[39,40] Importantly, El Fahime and colleagues[45] reported that forced expression of MMP-2 in normal myoblasts significantly increased migration of myoblasts *in vivo*. In the present study, we demonstrated that CD31(−) CD45(−) SP cells highly express MMP-2 (see Figure 7A and Supplementary Table S1 at *http://ajp.amjpathol.org*). Gelatin zymography confirmed that CD31(−) CD45(−) SP cells have high gelatinolytic activities (Figure 7B). Importantly, CD31(−) CD45(−) SP cells prepared from wild-type mice promoted the migration of transplanted myoblasts, but those from MMP-2-null mice did not (Figure 7C). Our results suggest that CD31(−) CD45(−) SP cells promote the migration of myoblasts via MMP-2 secretion. CD31(−) CD45(−) SP cells highly express MMP-2, 3, 9, 14, and 23 during regenerating muscle (see Supplementary Figures S1 and S2 and Supplementary Table S1 at *http://ajp.amjpathol.org*). Therefore, it remains to be determined whether MMPs other than MMP-2 also promote the migration of myoblasts. MMPs are reported to promote cell proliferation by releasing local growth factors stored within the extracellular matrix and process growth factor receptors.[34,35,46] In the present study, however, MMP-2 derived from CD31(−) CD45(−) SP cells did not stimulate the proliferation of myoblasts *in vivo* (Figure 7D). The factors that stimulate the proliferation of myoblasts remain to be determined in a future study. MMP-3, -9, -14, and -23 are candidates that play a role in stimulating the proliferation of myoblasts.

CD31(−) CD45(−) SP Cells Are the Third Cellular Component of Muscle Regeneration

Our results suggest that transplanted CD31(−) CD45(−) SP cells stimulate myogenesis of co-transplanted myoblasts by supporting their proliferation and migration. Our results also suggest that endogenous CD31(−) CD45(−) SP cells promote muscle regeneration by the same mechanisms. Muscle regeneration is a complex, highly coordinated process in which not only myogenic cells but also inflammatory cells such as macrophages play critical roles.[3] Based on our finding that CD31(−) CD45(−) SP cells regulate myoblast proliferation and migration, we

propose that CD31(−) CD45(−) SP cells are a third cellular component of muscle regeneration. In addition, gene expression analysis on CD31(−) CD45(−) SP cells revealed that CD31(−) CD45(−) SP cells express a wide range of regulatory molecules implicated in embryonic development, tissue growth and repair, angiogenesis, and tumor progression, suggesting that CD31(−) CD45(−) SP cells are a versatile player in regeneration of skeletal muscle. Future studies of ablation of endogenous CD31(−) CD45(−) SP cells in the mouse will likely further clarify the mechanisms by which CD31(−) CD45(−) SP cells promote muscle regeneration.

Acknowledgments

We thank Satoru Masuda and Chika Harano for technical support.

References

1. Chargé SB, Rudnicki MA: Cellular and molecular regulation of muscle regeneration. Physiol Rev 2004, 84:209–238
2. Orimo S, Hiyamuta E, Arahata K, Sugita H: Analysis of inflammatory cells and complement C3 in bupivacaine-induced myonecrosis. Muscle Nerve 1991, 14:515–520
3. Tidball JG: Inflammatory processes in muscle injury and repair. Am J Physiol 2005, 288:R345–R353
4. Mauro A: Satellite cell of skeletal muscle fibers. J Biophys Biochem Cytol 1961, 9:493–495
5. Collins CA, Olsen I, Zammit PS, Heslop L, Petrie A, Partridge TA, Morgan JE: Stem cell function, self-renewal, and behavioral heterogeneity of cells from the adult muscle satellite cell niche. Cell 2005, 122:289–301
6. Kuang S, Kuroda K, Le Grand F, Rudnicki MA: Asymmetric self-renewal and commitment of satellite stem cells in muscle. Cell 2007, 129:999–1010
7. Qu-Petersen Z, Deasy B, Jankowski, R, Ikezawa M, Cummins J, Pruchnic R, Mytinger J, Cao B, Gates C, Wernig A, Huard J: Identification of a novel population of muscle stem cells in mice: potential for muscle regeneration. J Cell Biol 2002, 157:851–864
8. Jiang Y, Vaessen B, Lenvik T, Blackstad M, Reyes M, Verfaillie CM: Multipotent progenitor cells can be isolated from postnatal murine bone marrow, muscle, and brain. Exp Hematol 2002, 30:896–904
9. Tamaki T, Akatsuka A, Ando K, Nakamura Y, Matsuzawa H, Hotta T, Roy RR, Edgerton VR: Identification of myogenic-endothelial progenitor cells in the interstitial spaces of skeletal muscle. J Cell Biol 2002, 157:571–577
10. Torrente Y, Tremblay JP, Pisati F, Belicchi M, Rossi B, Sironi M, Fortunato F, El Fahime M, D'Angelo MG, Caron NJ, Constantin G, Paulin D, Scarlato G, Bresolin N: Intraarterial injection of muscle-derived CD34(+)Sca-1(+) stem cells restores dystrophin in mdx mice. J Cell Biol 2001, 152:335–348
11. Polesskaya A, Seale P, Rudnicki MA: Wnt signaling induces the myogenic specification of resident CD45+ adult stem cells during muscle regeneration. Cell 2003, 113:841–852
12. Sampaolesi M, Blot S, D'Antona G, Granger N, Tonlorenzi R, Innocenzi A, Mognol P, Thibaud JL, Galvez BG, Barthelemy I, Perani L, Mantero S, Guttinger M, Pansarasa O, Rinaldi C, Cusella De Angelis MG, Torrente Y, Bordignon C, Bottinelli R, Cossu G: Mesoangioblast stem cells ameliorate muscle function in dystrophic dogs. Nature 2006, 444:574–579
13. Dellavalle A, Sampaolesi M, Tonlorenzi R, Tagliafico E, Sacchetti B, Perani L, Innocenzi A, Galvez BG, Messina G, Morosetti R, Li S, Belicchi M, Peretti G, Chamberlain JS, Wright WE, Torrente Y, Ferrari S, Bianco P, Cossu G: Pericytes of human skeletal muscle are myogenic precursors distinct from satellite cells. Nat Cell Biol 2007, 9:255–267
14. Goodell MA, Brose K, Paradis G, Conner AS, Mulligan RC: Isolation and functional properties of murine hematopoietic stem cells that are replicating in vivo. J Exp Med 1996, 183:1797–1806
15. Gussoni E, Soneoka Y, Strickland CD, Buzney EA, Khan MK, Flint AF, Kunkel LM, Mulligan RC: Dystrophin expression in the mdx mouse restored by stem cell transplantation. Nature 1999, 401:390–394
16. Jackson KA, Mi T, Goodell MA: Hematopoietic potential of stem cells isolated from murine skeletal muscle. Proc Natl Acad Sci USA 1999, 96:14482–14486
17. Asakura A, Seale P, Girgis-Gabardo A, Rudnicki MA: Myogenic specification of side population cells in skeletal muscle. J Cell Biol 2002, 159:123–134
18. Bachrach E, Perez AL, Choi YH, Illigens BM, Jun SJ, del Nido P, McGowan FX, Li S, Flint A, Chamberlain J: Muscle engraftment of myogenic progenitor cells following intraarterial transplantation. Muscle Nerve 2006, 34:44–52
19. Frank NY, Kho AT, Schatton T, Murphy GF, Molloy MJ, Zhan Q, Ramoni MF, Frank MH, Kohane IS, Gussoni E: Regulation of myogenic progenitor proliferation in human fetal skeletal muscle by BMP4 and its antagonist Gremlin. J Cell Biol 2006, 175:99–110
20. Uezumi A, Ojima K, Fukada S, Ikemoto M, Masuda S, Miyagoe-Suzuki Y, Takeda S: Functional heterogeneity of side population cells in skeletal muscle. Biochem Biophys Res Commun 2006, 341:864–873
21. Ojima K, Uezumi A, Miyoshi H, Masuda S, Morita Y, Fukase A, Hattori A, Nakauchi H, Miyagoe-Suzuki Y, Takeda S: Mac-1(low) early myeloid cells in the bone marrow-derived SP fraction migrate into injured skeletal muscle and participate in muscle regeneration. Biochem Biophys Res Commun 2004, 321:1050–1061
22. Itoh T, Ikeda T, Gomi H, Nakao S, Suzuki T, Itohara S: Unaltered secretion of β-amyloid precursor protein in gelatinase A (matrix metalloproteinase 2)-deficient mice. J Biol Chem 1997, 272:22389–22392
23. Fukada S, Higuchi S, Segawa M, Koda K, Yamamoto Y, Tsujikawa K, Kohama Y, Uezumi A, Imamura M, Miyagoe-Suzuki Y, Takeda S, Yamamoto H: Purification and cell-surface marker characterization of quiescent satellite cells from murine skeletal muscle by a novel monoclonal antibody. Exp Cell Res 2004, 296:245–255
24. Kitamura T, Koshino Y, Shibata F, Oki T, Nakajima H, Nosaka T, Kumagai H: Retrovirus-mediated gene transfer and expression cloning: powerful tools in functional genomics. Exp Hematol 2003, 31:1007–1014
25. Morita S, Kojima T, Kitamura T: Plat-E: an efficient and stable system for transient packaging of retroviruses. Gene Ther 2000, 7:1063–1066
26. Lee SJ, McPherron AC: Regulation of myostatin activity and muscle growth. Proc Natl Acad Sci USA 2001, 98:9306–9311
27. Holly J, Perks C: The role of insulin-like growth factor binding proteins. Neuroendocrinology 2006, 83:154–160
28. Sakamoto K, Yamaguchi S, Ando R, Miyawaki A, Kabasawa Y, Takagi M, Li CL, Perbal B, Katsube K: The nephroblastoma overexpressed gene (NOV/ccn3) protein associates with Notch1 extracellular domain and inhibits myoblast differentiation via Notch signaling pathway. J Biol Chem 2002, 277:29399–29405
29. Lawler J: The functions of thrombospondin-1 and-2. Curr Opin Cell Biol 2000, 12:634–640
30. Tocharus J, Tsuchiya A, Kajikawa M, Ueta Y, Oka C, Kawaichi M: Developmentally regulated expression of mouse HtrA3 and its role as an inhibitor of TGF-beta signaling. Dev Growth Differ 2004, 46:257–274
31. Colarossi C, Chen Y, Obata H, Jurukovski V, Fontana L, Dabovic B, Rifkin DB: Lung alveolar septation defects in Ltbp-3-null mice. Am J Pathol 2005, 167:419–428
32. McCawley LJ, Matrisian LM: Matrix metalloproteinases: they're not just for matrix anymore! Curr Opin Cell Biol 2001, 13:534–540
33. Balcerzak D, Querengesser L, Dixon WT, Baracos VE: Coordinate expression of matrix-degrading proteinases and their activators and inhibitors in bovine skeletal muscle. J Anim Sci 2001, 79:94–107
34. Kayagaki N, Kawasaki A, Ebata T, Ohmoto H, Ikeda S, Inoue S, Yoshino K, Okumura K, Yagita H: Metalloproteinase-mediated release of human Fas ligand. J Exp Med 1995, 182:1777–1783
35. Lanzrein M, Garred O, Olsnes S, Sandvig K: Diphtheria toxin endocytosis and membrane translocation are dependent on the intact membrane-anchored receptor (HB-EGF precursor): studies on the cell-associated receptor cleaved by a metalloprotease in phorbol-ester-treated cells. Biochem J 1995, 310:285–289
36. Couch CB, Strittmatter WJ: Rat myoblast fusion requires metalloendoprotease activity. Cell 1983, 32:257–265

37. Ohtake Y, Tojo H, Seiki M: Multifunctional roles of MT1-MMP in myofiber formation and morphostatic maintenance of skeletal muscle. J Cell Sci 2006, 119:3822–3832
38. Kherif S, Lafuma C, Dehaupas M, Lachkar S, Fournier JG, Verdière-Sahuqué M, Fardeau M, Alameddine HS: Expression of matrix metalloproteinases 2 and 9 in regenerating skeletal muscle: a study in experimentally injured and mdx muscles. Dev Biol 1999, 205:158–170
39. Fukushima K, Nakamura A, Ueda H, Yuasa K, Yoshida K, Takeda S, Ikeda S: Activation and localization of matrix metalloproteinase-2 and -9 in the skeletal muscle of the muscular dystrophy dog (CXMDJ). BMC Musculoskelet Disord 2007, 8:54
40. von Moers A, Zwirner A, Reinhold A, Brückmann O, van Landeghem F, Stoltenburg-Didinger G, Schuppan D, Herbst H, Schuelke M: Increased mRNA expression of tissue inhibitors of metalloproteinase-1 and -2 in Duchenne muscular dystrophy. Acta Neuropathol (Berl) 2005, 109:285–293
41. Pittenger MF, Mackay AM, Beck SC, Jaiswal RK, Douglas R, Mosca JD, Moorman MA, Simonetti DW, Craig S, Marshak DR: Multilineage potential of adult human mesenchymal stem cells. Science 1999, 284:143–147
42. Conget PA, Minguell JJ: Phenotypical and functional properties of human bone marrow mesenchymal progenitor cells. J Cell Physiol 1999, 181:67–73
43. Caplan AI, Dennis JE: Mesenchymal stem cells as trophic mediators. J Cell Biochem 2006, 98:1076–1084
44. Oh J, Takahashi R, Adachi E, Kondo S, Kuratomi S, Noma A, Alexander DB, Motoda H, Okada A, Seiki M, Itoh T, Itohara S, Takahashi C, Noda M: Mutations in two matrix metalloproteinase genes, MMP-2 and MT1-MMP, are synthetic lethal in mice. Oncogene 2004, 23:5041–5048
45. El Fahime E, Torrente Y, Caron NJ, Bresolin MD, Tremblay JP: In vivo migration of transplanted myoblasts requires matrix metalloproteinase activity. Exp Cell Res 2000, 258:279–287
46. Gearing AJ, Beckett P, Christodoulou M, Churchill M, Clements J, Davidson AH, Drummond AH, Galloway WA, Gilbert R, Gordon JL, Leber TM, Mangan M, Miller K, Nayee P, Owen K, Patel S, Thomas W, Wells G, Wood LM, Woolley K: Processing of tumour necrosis factor-alpha precursor by metalloproteinases. Nature 1994, 370:555–557

Water-dispersed single-wall carbon nanohorns as drug carriers for local cancer chemotherapy

Tatsuya Murakami[1,2], Hirohide Sawada[1], Goshu Tamura[3], Masako Yudasaka[2,4], Sumio Iijima[2,3,4] & Kunihiro Tsuchida[1†]

†Author for correspondence
[1]Institute for Comprehensive Medical Science, Fujita Health University, Toyoake, Aichi 470-1192, Japan
Tel.: +81 562 939 384; Fax: + 81 562 935 791; E-mail: tsuchida@fujita-hu.ac.jp
[2]SORST/JST, c/o NEC, 34 Miyukigaoka, Tsukuba, Ibaraki 305-8501, Japan
[3]Meijo University, 1–501 Shiogamaguchi, Tenpaku, Nagoya 468-8502, Japan
[4]NEC, 34 Miyukigaoka, Tsukuba, Ibaraki 305-8501, Japan

Aim: Functional analyses of water-dispersed carbon nanohorns with antitumor activity were performed to explore their potential as a drug carrier for local cancer chemotherapy. **Materials & methods:** Water-dispersed carbon nanohorns were prepared through adsorption of polyethylene glycol-doxorubicin conjugate (PEG–DXR) onto oxidized single-wall carbon nanohorns (oxSWNHs). PEG–DXR-bound oxSWNHs were administered intratumorally to human nonsmall cell lung cancer-cell NCI-H460-bearing mice. **Results & discussion:** When injected intratumorally, PEG–DXR-bound oxSWNHs caused significant retardation of tumor growth associated with prolonged DXR retention in the tumor. In accordance with this DXR retention, a large number of oxSWNH agglomerates was found in the periphery of the tumor. Histological analyses showed migration of oxSWNHs to the axillary lymph node, which is a major site of breast cancer metastasis near the tumor, possibly by means of interstitial lymphatic-fluid transport. **Conclusions:** These results suggest that water-dispersed oxSWNHs may thus be useful as a drug carrier for local chemotherapy.

Drug delivery systems are designed to improve the pharmacological and therapeutic properties of drugs administered intravascularly or interstitially and include particulate carriers that can function as drug reservoirs. Among such particulate drug carriers, liposomes and lipid microspheres have been approved for the treatment of cancers [1], arterial occlusive diseases [2] and others [3,4]. Polymer micelles conjugated with anticancer drugs are in clinical trials currently [5]. In addition, recent advances in nanotechnology and nanofabrication enable the production of various nanoparticles as attractive drug carriers. For example, gold nanoparticles are suitable not only for adsorbing an anticancer drug, cisplatin, on the surface, but also for performing near-infrared light-dependent release of cisplatin [6].

Recently, single-wall carbon nanohorns (SWNHs) [7] were discovered as nanoaggregates composed of single-wall carbon nanotubes with closed ends (**Figure 1A**). The mean diameter of SWNHs is approximately 80–100 nm and each tube has a mean diameter of 2–3 nm. Oxidized carbon nanohorns (oxSWNHs) have nm-sized pores (<2 nm) in the walls of each carbon nanotube (**Figure 1A, lower**) [8]. In contrast to carbon nanotubes, SWNHs as well as oxSWNHs can be prepared without any metals, such as iron. Importantly, Miyawaki *et al.* reported recently that SWNHs are a nonirritant and a nondermal sensitizer in rabbits and rarely damage rat lung after intratracheal instillation, whereas carbon nanotubes cause foreign-body granuloma in rat lung [9]. OxSWNHs have been recognized as a new class of drug carrier. The deposition of dexamethasone [10] or cisplatin [11] into the tube interior space of oxSWNHs and the adsorption of a polyethylene glycol-doxorubicin conjugate (PEG–DXR) on the outer surface of oxSWNHs [12] have been reported previously. In the latter case, oxSWNHs were dispersed simultaneously in aqueous solution owing to the action of the PEG moiety through physical adsorption of the DXR moiety of PEG–DXR (**Figure 1B**). This was supported by the observation that co-treatment of oxSWNHs with PEG–DXR and DXR inhibited the water dispersion of oxSWNHs [12].

Water-dispersed oxSWNHs (PEG–DXR–oxSWNHs) are of special interest because of possible biochemical and biomedical applications [13]. Furthermore, water-dispersed amino-SWNHs [14] as well as as-prepared oxSWNHs [11] did not show obvious cytotoxicity *in vitro*, whereas cytotoxicity of carbon nanotubes is still controversial [15,16]. However, metabolism, excretion and long-term effects of water-dispersed carbon nanomaterials in the body are not understood fully [17,18], whereas intravenously administered carbon nanotubes were reportedly excreted from the main organs, in which they accumulated, in 2 months [13]. Thus, the *in vivo* application of carbon nanotubes should be undertaken carefully. In fact, water-dispersed oxSWNHs used in this study were found in the reticuloendothelial system even 1 month after their

Keywords: axillary lymph node, carbon nanohorn, conjugate, doxorubicin, local chemotherapy, lymphatic delivery, PEGylation

10.2217/17435889.3.4.453 © 2008 Future Medicine Ltd ISSN 1743-5889

Figure 1. Structures of oxSWNH and PEG–DXR–oxSWNH.

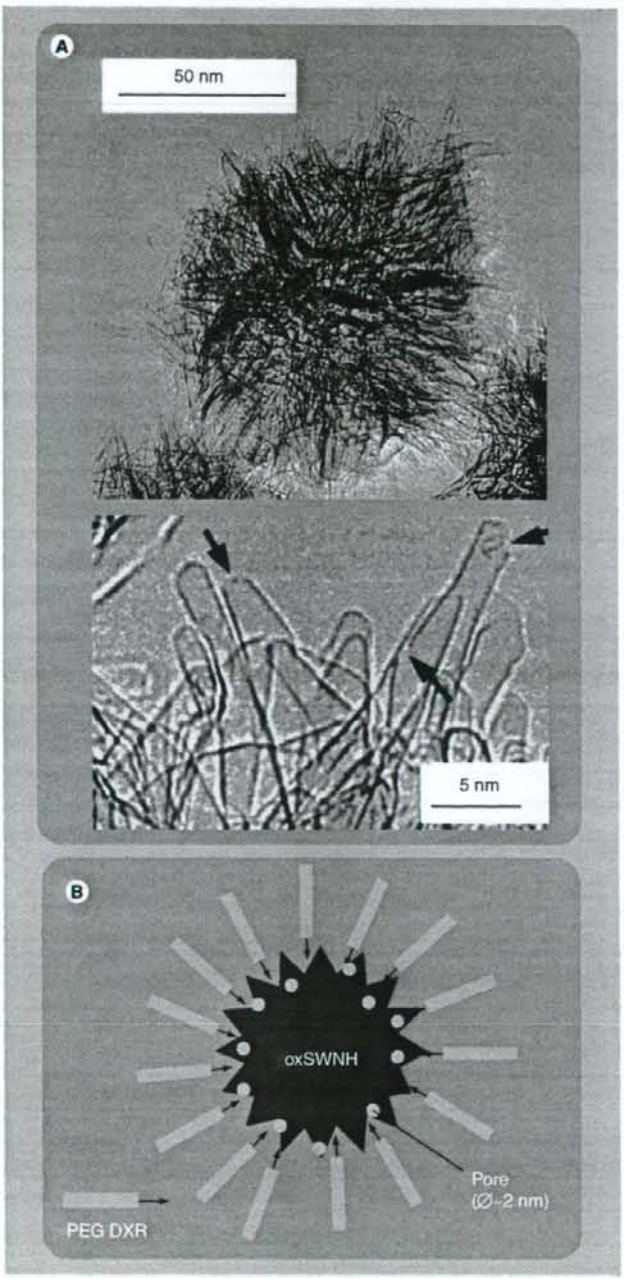

(A) TEM image of an oxSWNH: the whole image (*upper*) and the surface image (*lower*). OxSWNHs have nm-sized pores (<2 nm) in the walls of each carbon nanotube (arrow in A, *lower*). **(B)** Drawing of PEG–DXR–oxSWNH.
DXR: Doxorubicin; oxSWNH: Oxidized carbon nanohorn; PEG: Polyethylene glycol; TEM: Transmission-electron microscope.

intravenous administration in mice (Figure 2C & 2F). When taking a closer look at the images, oxSWNH agglomerates were colocalized with F4/80-positive cells, macrophages, in both liver (Figure 2B & 2C) and spleen (Figure 2E & 2F), suggesting uptake in the reticuloendothelial system. Histologically, an acute inflammatory infiltrate was not obvious. For *in vivo* functional analyses of PEG–DXR– oxSWNHs, therefore, local injection of PEG–DXR–oxSWNHs was performed to minimize their potential adverse effects.

The rationale for local chemotherapy is that the tumor receives sustained exposure to a high concentration of antitumor drugs whereas normal tissues are relatively spared. Importantly, the effectiveness of intraperitoneal administration of anticancer drugs was reported recently in ovarian [19] and gastric cancers [20,21]. It should be noted that, in some cases, drug carriers contributed to the effectiveness [22,23]. Here, fundamental *in vitro* and *in vivo* properties of PEG–DXR–oxSWNHs are presented to discuss the possibility of PEG–DXR-oxSWNH as a drug carrier for local chemotherapy.

Materials & methods

Materials

Dahlia-like SWNHs were synthesized by CO_2 laser ablation of graphite under Ar gas at 101 kPa. SWNHs used in this study contain carbonaceous byproducts, named giant graphitic balls [24], at 5%. Their oxidized form, oxSWNHs, were prepared as described previously [8,25]. Briefly, as-grown SWNHs prepared by laser ablation were oxidized for 10 min in oxygen (760 Torr) at 580°C and were then heated at 400°C for an additional 2 h under ultra-high vacuum (~1×10^{-7} Torr).

Doxorubicin hydrochloride (DXR) was from Wako (Osaka, Japan). Poly(oxyethylene)sorbitan monolaurate (Tween®20, molecular biology tested) was from SIGMA-Aldrich (St. Louis, MO, USA). 1-Ethyl-3-(3-dimethylaminopropyl)-carbodiimide, hydrochloride and Cell Counting Kit-8 were from Dojindo Laboratories (Kumamoto, Japan). *In situ* cell death detection kit, TMR red, was from Roche Molecular Biochemicals (Mannheim, Germany). TSK-GEL ODS-100S (4.6 × 150 mm) was from TOSOH (Tokyo, Japan). Sephadex™ G-50 Medium and PD-10 columns were purchased from GE Healthcare UK Ltd (Buckinghamshire, UK). Fetal bovine serum (FBS) was from Japan Bioserum (Hiroshima, Japan). Roswell Park Memorial Institute (RPMI, NY, USA) 1640, Dulbecco's phosphate-buffered

Figure 2. Long-term retention of oxSWNH agglomerates in the reticuloendothelial system.

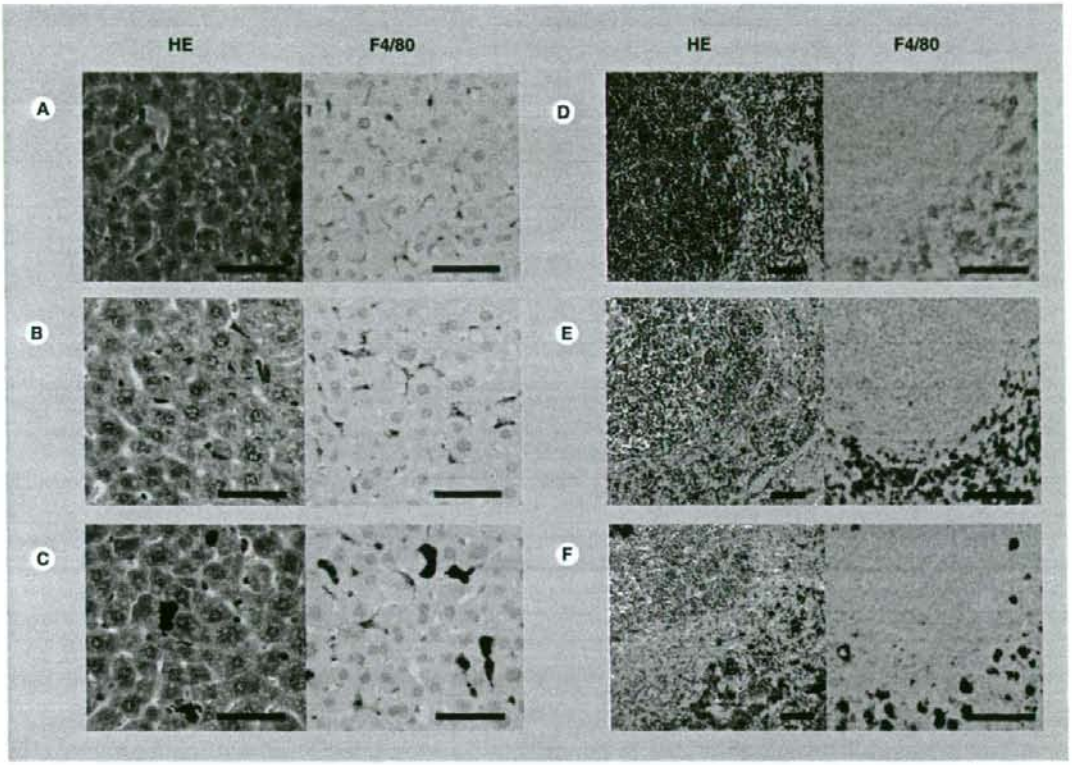

HE and immunohistochemical analyses of the liver and spleen excised from BALB/c mice after intravenous administration of PEG–DXR–oxSWNH (20 k PEG) at a dose of 10 mg/kg on an oxSWNH basis; liver after 1 **(B)** and 42 days **(C)** and spleen after 1 **(E)** and 42 days **(F)**. Liver **(A)** and spleen **(D)** of untreated mice are also shown. OxSWNH agglomerates remained mostly in macrophages (F4/80$^+$ cells in right panels, *brown*) of liver and spleen over 1 month, whereas infiltration of monocytes, indicative of inflammation, was not obvious in liver. Scale bar = 50 μm.
DXR: Doxorubicin; HE: Hematoxylin and eosin; oxSWNH: Oxidized carbon nanohorn; PEG: Polyethylene glycol.

saline, trypsin–EDTA (0.05% trypsin, 0.53 mM EDTA-4Na), penicillin and streptomycin were from Invitrogen (Carlsbad, CA). Cell-culture dishes and Matrigel™ Basement Membrane Matrix were from BD Bioscience (San Jose, CA, USA).

Animals

A selection of 5 week-old male mice (BALB/c) and immunodeficient, 4 week-old athymic nude female mice (BALB/c *nu/nu*) were purchased from CLEA (CLEA Japan Inc., Tokyo, Japan) and housed in a specific pathogen-free animal facility at Fujita Health University in accordance with the regulations of the University's committee on the Use and Care of Animals. Animals were fed *ad libitum* with γ-irradiated rodent diet CE2 (CLEA Japan Inc.).

Preparation of PEG–DXR

100 mg of 5 k PEG-succinimidylsuccinate (PEG; average molecular weight 5,000) and 14 mg of DXR (1.5 mol equiv.) were dissolved in 4 ml of dry *N,N'*-dimethylformamide (DMF) and 5 ml of dry DMF containing 3.2 μl of triethylamine, respectively. The DXR solution was then added drop-wise to the PEG solution with stirring, after which the reaction mixture was stirred under shielding from light at room temperature for 6 days. Triethylamine (2.3 μl) and 1-ethyl-3-(3-dimethylaminopropyl)-carbodiimide, hydrochloride (3.8 mg) were added to the reaction mixture once per day. The PEG–DXR produced was monitored by a reversed-phase LC-10A high-performance liquid chromatography (Shimadzu, Kyoto, Japan) on a

Table 1. *In vitro* growth inhibition of free DXR, free PEG-DXR and PEG-DXR-oxSWNH against NCI-H460 cells.

Basis	IC_{50} (μg/ml)		
	DXR	*PEG–DXR*	*PEG–DXR–oxSWNH*
oxSWNH	–	–	33 ± 4.0
PEG–DXR	–	1.6 ± 0.2	7.9*
DXR	0.0085	0.17*	0.82*

*Calculated mean values from their actual mean values based on PEG–DXR content in PEG–DXR–oxSWNH and PEG molecular weight of PEG-DXR.
DXR: Doxorubicin; IC: Median inhibitory concentration; oxSWNH: Oxidized single-walled carbon nanohorn;
PEG–DXR: Polyethylene glycol-doxorubicin conjugate; PEG–DXR–oxSWNH: Water-dispersed oxidized single-wall carbon nanohorn.

TKS-GEL ODS-100S column with a 20 mM triethylamine formate (pH 2.8)/acetonitrile gradient. A ninefold volume of diethyl ether was poured into the reaction mixture with stirring, resulting in precipitation of PEG derivatives. The precipitates were collected by centrifugation and redissolved in a small amount of water. PEG–DXR in this aqueous solution was further purified using a water-equilibrated G-50 gel filtration column (ø 1.5 cm × 18 cm). PEG–DXR was eluted with water, after which the eluate was freeze-dried.

Preparation of PEG–DXR–oxSWNHs

The procedure reported previously for the preparation of PEG–DXR–oxSWNHs was modified slightly as follows. OxSWNHs were suspended in ethanol (0.2 mg/ml), after which the solution was sonicated in a glass vial at the bottom of the water bath of a Bransonic Tabletop Ultrasonic Cleaner 8510J-MT (Branson Ultrasonic Corporation, Danbury, CT, USA) for 35 min. The ethanol solution of oxSWNHs was cooled on ice and diluted 1:1 with stirring by drop-wise addition of PEG–DXR solution (0.8 mg/ml) in H_2O sterilized by membrane filtration. The mixture was stirred on ice for 2 h and then concentrated to less than half of the starting volume under vacuum. After incubation at 4°C overnight, the concentrated reaction mixture was allowed to pass through a PD-10 column, a gel filtration column for desalting. Free PEG–DXR in the filtrate was removed by washing four times with an Amicon Ultra ultrafiltration device (100 kDa molecular weight cut-off) [12]. The amount of bound PEG–DXR within the complexes was calculated to be 240 mg of PEG–DXR per g of oxSWNH by the method reported previously [12].

Histological analysis

Tumors, livers and spleens were isolated from mice administered PEG–DXR–oxSWNH intravenously and were fixed in 4% paraformaldehyde overnight. The tissues were then processed for paraffin embedding. Multiple 3 μm-thick microtome sections from each tissue were dewaxed, hydrated and stained with hematoxylin and eosin (HE) by the standard method. For immunohistochemical staining, these sections were dewaxed and hydrated and treated with 0.1 mg/ml trypsin at 37°C for 30 min for antigen retrieval. Macrophage glycoprotein F4/80 was detected in the sections by rat monoclonal anti-F4/80 IgG (BMA Biomedicals, Augst, Switzerland).

Cell culture

NCI-H460 human nonsmall cell lung cancer cells were purchased from the National Cancer Institute (Frederick, MD, USA) and were maintained in RPMI1640 supplemented with 5% FBS, 100 U/ml penicillin and 100 μg/ml streptomycin. Cells were incubated at 37°C under a humidified atmosphere of 5% CO_2 and 95% air and were passaged every 3–4 days.

In vitro *antitumor activity*

NCI-H460 cells (2.5×10^3 cells in 100 μl of medium) were seeded into 96-well plates and cultured for 4 h at 37°C to attach the plates, after which the medium was substituted carefully with fresh media containing PEG–DXR–oxSWNH. Because NCI-H460 cells grow quickly to become confluent, this immediate medium change enabled long treatment of the cells with the samples for sensitization in cell-viability testing. After culturing for 72 h at 37°C with PEG–DXR–oxSWNH, cell viabilities were evaluated by a Cell Counting Kit-8 and a Multiscan JX microplate reader (Thermo Fisher Scientific, Inc., Waltham, MA, USA). Cell viabilities were normalized to (OD_{450}–OD_{630}) for the untreated cells. Assays were performed in triplicate determination. The median inhibitory concentration (IC_{50}) was calculated based on cell viabilities.

In vivo *antitumor activity*

NCI-H460 cells were harvested with trypsin–EDTA solution, washed and resuspended in a 1:1 mixture of RPMI1640 and Matrigel™. The cell suspension (1.0×10^6 cells in 50 µl) was injected subcutaneously (s.c.) into the left flank of each mouse using a 26 gauge needle. The tumors were allowed to grow for 1 week until reaching approximately 100 mm^3. Then, the mice were treated intratumorally (i.t.) three times at 4-day intervals either with PEG–DXR (n = 4) at a dose of 1.2 mg/kg or PEG–DXR–oxSWNH (n = 5) at a dose of 1.2 mg/kg on a PEG–DXR basis. When i.t. was administered with PEG–DXR–oxSWNH at a higher dose (4.8 mg/kg), no enhancement of the antitumor activity was observed. Although the reasons for this remain unclear, the dose of 1.2 mg/kg was chosen to minimize the potential adverse effects. The size of the tumors was measured immediately before each treatment using hand-held calipers along the longest width (W) and the corresponding perpendicular length (L). The formula chosen to compute tumor volume (V) was $V = ½ \times L \times W^2$. The tumor growth rate was calculated based on the formula:

volume of the tumor at the point of measurement/volume of the tumor on the first day of treatment.

Two-sided Student's t-test was used to compare the means of the PEG–DXR-treated group and the PEG–DXR–oxSWNH-treated group. The statistical significance was set at $p < 0.05$.

Doxorubicin concentration in tumor tissue & plasma

Tumor tissues were excised from NCI-H460-bearing mice and weighed. After addition of a threefold weight of 10% SDS in phosphate-buffered saline, the tumor tissues were homogenized with Disperser T 10 basic (IKA, Staufen, Germany). The tumor homogenates were centrifuged at 13,500 rpm for 10 min at room temperature. The supernatants (100 µl) were heated at 50°C for 2 h in the presence of 1 N HCl to enable both PEG–DXR and DXR in the supernatant to decompose to doxorubicinon [26]. After neutralization by 1 M Tris, the acid-treated samples were freeze-dried. The samples were resuspended in DMF and then sonicated for 10 min. The DMF suspensions were centrifuged at 16,500 g for 10 min and the supernatants were subjected to a reversed-phase LC-10A high-performance liquid chromatography (Shimadzu, Kyoto, Japan) on a TKS-GEL ODS-100S column with a 20 mM triethylamine formate (pH 2.8)/acetonitrile gradient. Doxorubicinon was detected fluorescently (Ex/Em 485/558 nm) with a retention time of 8.1 min.

Blood samples (100 µl) were collected from the tail vein of the NCI-H460-bearing mice using a heparinized 75 mm hematocrit tube (Hemato-Clad, Drummond Scientific Company, Broomall, PA, USA) at the indicated times and immediately mixed with 100 µl of 0.1% EDTA in phosphate-buffered saline on ice to prevent hemolysis. The mixtures were centrifuged at 800 rpm for 5 min at 4°C. Doxorubicinon in the supernatants (100 µl) was analyzed by reverse-phase high-performance liquid chromatography (HPLC) after being heated in 1 N HCl as described earlier.

Results & discussion

Growth-inhibitory effect of PEG–DXR–oxSWNH in vitro

In the previous study, the induction of apoptosis in NCI-H460 by treatment with PEG–DXR–oxSWNH using terminal deoxynucleotidyl transferase-mediated dUTP–fluorescein nick-end

Table 2. Pharmacokinetic properties of DXR after intratumoral administration.

	PEG-DXR	PEG-DXR-oxSWNH
	Residual DXR in tumor tissue on day 21 (%)	
	0.57*	61 ± 25
Time (h)	***DXR in blood (ng/ml)***	
0.5	33 ± 10	10 ± 5.7
1	24 ± 6.3	8.3 ± 0.96
3	11 ± 4.7	4.2 ± 4.1
24	ND	ND

*Average of two mice in which DXR could be detected.

DXR: Doxorubicin; ND: Not detected; PEG–DXR: Polyethylene glycol-doxorubicin conjugate; PEG–DXR–oxSWNH: Water-dispersed oxidized single-wall carbon nanohorn.

Figure 3. *In vivo* effectiveness of PEG–DXR–oxSWNHs compared with PEG–DXR.

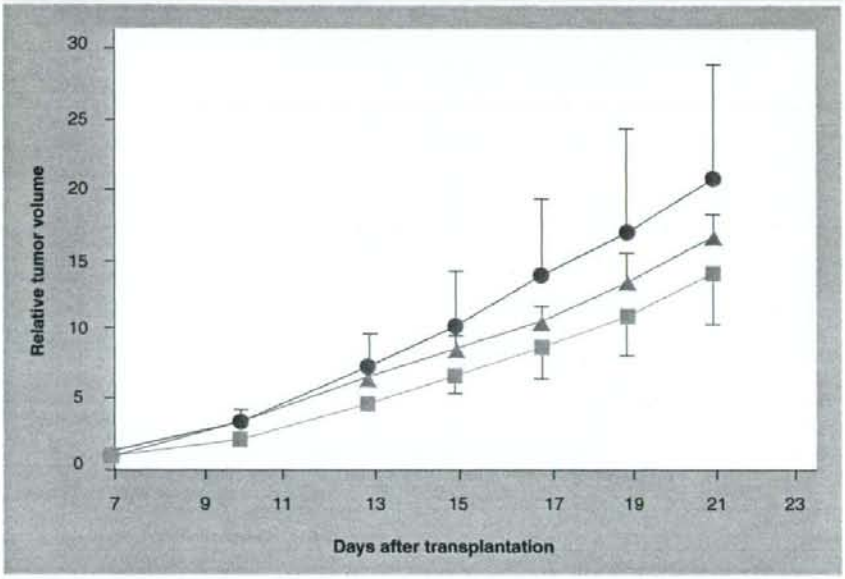

In vivo antitumor activity of PEG–DXR–oxSWNHs against NCI-H460 cells implanted subcutaneous in immunodeficient BALB/c nude mice (female, $n = 4$ or 5). Each drug was intratumoral administered three times on day 7, 11 and 15 (arrows) at the dose of 1.2 mg/kg on a PEG–DXR. Saline (●), PEG–DXR (▲) or PEG–DXR–oxSWNH (■). The tumor volume is expressed as mean. Scale bar ± SD.
DXR: Doxorubicin; oxSWNH: Oxidized carbon nanohorn; PEG: Polyethylene glycol; SD: Standard deviation.

labeling (TUNEL) staining was reported [12]. The median growth-inhibitory concentration of DXR against NCI-H460 cells was 0.0085 µg/ml. Here, the growth inhibitory effect of PEG–DXR–oxSWNH on cultured NCI-H460 cells was assessed before *in vivo* studies. Cell viability was determined after 72 h incubation in the presence of PEG–DXR or PEG–DXR–oxSWNHs. As shown in Table 1, IC_{50} of free PEG–DXR and PEG–DXR–oxSWNH against NCI-H460 cells is 1.6 ± 0.2 µg/ml and 33 ± 4.0 µg/ml, respectively. The average value for PEG–DXR–oxSWNH (33 µg/ml) corresponds to 7.9 µg/ml on a PEG–DXR basis and 0.82 µg/ml on a DXR basis. This is because PEG–DXR–oxSWNH contains 240 mg of PEG–DXR per gram of oxSWNH and the molecular weight of PEG used in this study is 5,000. These values are approximately 5 and 100 times higher than the value for free PEG–DXR (1.6 µg/ml) and free DXR (0.0085 µg/ml), respectively. In the case of free PEG–DXR, the IC_{50} was 20 times larger than the value of free DXR. These figures may reflect the fact that the DXR of PEG–DXR–oxSWNHs needs to be released from both PEG and the surface of the oxSWNHs to express its antitumor activity. In fact, PEG–DXR was detected almost exclusively by HPLC analysis of the supernatants from aqueous suspensions (pH 5–8) of PEG–DXR–oxSWNHs after incubation of the suspensions at 37°C for 4 and 24 h, while slightly increasing at acidic pH (data not shown). These also indicate that potentiation of the antitumor activity by linker refinement in PEG–DXR is needed.

Growth-inhibitory effect of PEG–DXR–oxSWNH in vivo

In vivo antitumor activity of PEG–DXR–oxSWNH was evaluated with s.c. NCI-H460-bearing nude mice by i.t. injection three times at intervals of 4 days. There are two reasons for selecting the i.t. route, as follows. First, another type of carbon nanoparticle, charcoal particles, which are dispersed in water by polymer wrapping, have been administered locally to cancer patients as black dyes to detect lymphatic metastasis of cancer [27]. Locally administered charcoals can be resected surgically with the

tumor tissue. Second, oxSWNH agglomerates deposited in liver and spleen for at least 1 month when PEG–DXR–oxSWNHs were administered intravenously to mice (Figure 2). Thus, the oxSWNH prepared in this study is not excreted easily from the body. Therefore, the i.t. route of administration was selected for the evaluation of *in vivo* antitumor activity of PEG–DXR–oxSWNHs.

Although the IC_{50} of PEG–DXR–oxSWNH toward NCI-H460 cells is higher than that of PEG–DXR (Table 1), PEG–DXR–oxSWNH suppressed tumor growth more effectively than PEG–DXR up to day 13 ($p < 0.05$). No weight loss either in PEG–DXR- or PEG–DXR–oxSWNH-treated groups was observed compared with an untreated control group during this period (data not shown). As described in the next section, this *in vivo* effectiveness of PEG–DXR–oxSWNHs is probably a result of the tight binding of PEG–DXR to oxSWNH.

Prolonged retention of DXR after intratumoral administration of PEG–DXR–oxSWNHs

The amount of DXR remaining in the tumor tissue on day 21 was estimated after three times' i.t. administration of PEG–DXR–oxSWNHs. Each tumor tissue was homogenized and treated with 1 N HCl to decompose PEG–DXR and its DXR derivatives into doxorubicinon [26], which was quantified by HPLC analysis. In the case of PEG–DXR administration, DXR was detected only in two out of four mice and on average accounted for 0.57% of the total amount of administered PEG–DXR (Table 2). By contrast to this, the tumor tissues of PEG–DXR–oxSWNH-treated mice retained 61% on a DXR basis. This high DXR retention ability of oxSWNH would provide longer exposure of the tumor to DXR.

To further confirm the increased retention of DXR and its derivatives in tumors by oxSWNHs, we examined a time course of the

Figure 4. Appearance and HE analysis of the tumor xenografts and adjacent lymph nodes excised from BALB/c nude mice treated with PEG–DXR–oxSWNH.

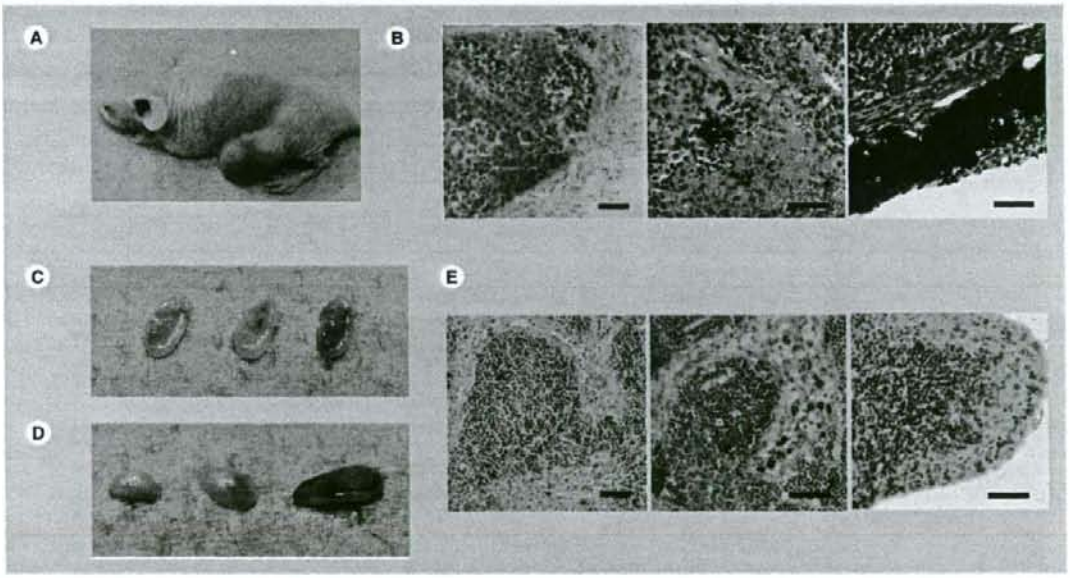

(A) A representative photograph of the mouse to which PEG–DXR–oxSWNHs were i.t. administered. **(B)** Representative images of NCI–H460–s.c. xenografts isolated on day 21 from mice treated with PEG–DXR–oxSWNHs are shown; untreated tumor (left), the middle (middle) and periphery (right) of the treated tumor. **(C)** Photographs of axillary lymph nodes isolated on day 28 from mice treated with saline (left), PEG–DXR (middle) or PEG–DXR–oxSWNH (right) are shown. **(D)** Photographs of inguinal (left), brachial (middle) and axillary lymph node (right) isolated on day 36 from mice treated with PEG–DXR–oxSWNH are shown. **(E)** HE analysis of the axillary lymph node isolated on day 36 from mice treated with PEG–DXR–oxSWNH was also performed; control axillary lymph node (left), the center (middle) and periphery (right) of the axillary lymph node. Scale bar = 50 μm.
DXR: Doxorubicin; HE: Hematoxylin and eosin; i.t.: Intratumoral; oxSWNH: Oxidized carbon nanohorn; PEG: Polyethylene glycol; s.c.: Subcutaneous.

Figure 5. TUNEL staining of tumor xenografts.

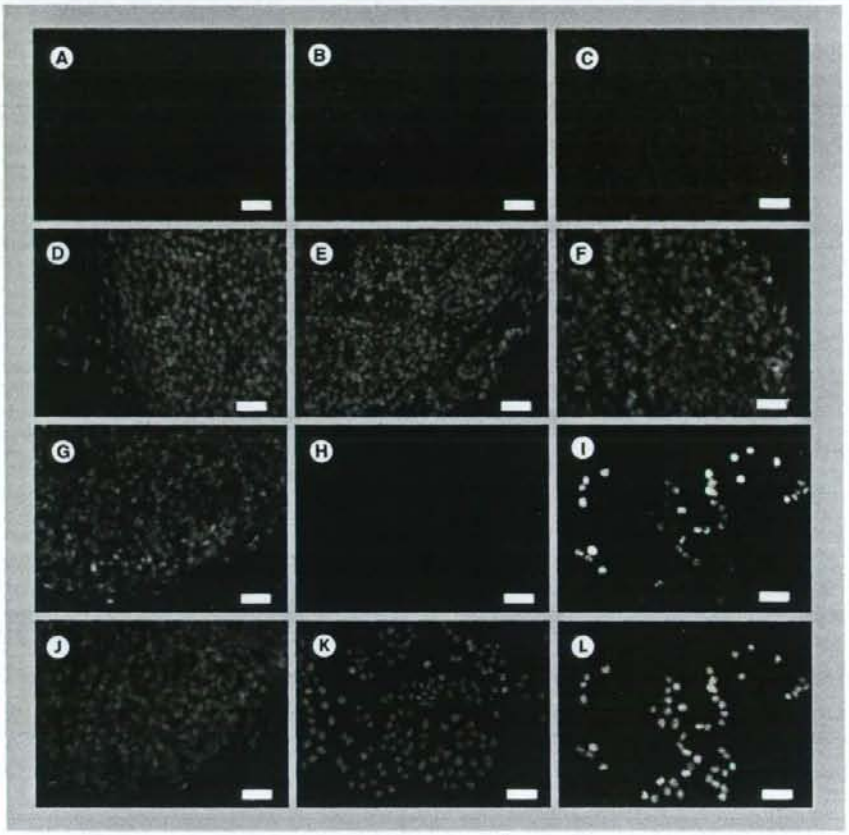

Fluorescent images of the tumor xenografts isolated on day 10 from BALB/c nude mice treated with saline **(A,G)**, PEG–DXR **(B,H)** or PEG–DXR–oxSWNH **(C,I)**. Treatment with DNase I is shown as a positive control **(D,J)**. The fixed tumor xenografts were processed and stained with TUNEL **(A–D)** and DAPI **(G–J)**. Cultured NCI–H460 cells were also stained with TUNEL **(E,F)** and DAPI **(K,L)** after treatment with **(F,L)** or without **(E,K)** PEG–DXR (0.2 μg/ml) for 3 days. Scale bar = 50 μm.
DAPI: 4',6-diamino-2-phenylindole; DXR: Doxorubicin; oxSWNH: Oxidized single-walled carbon nanohorn; PEG: Polyethylene glycol; TUNEL: Terminal deoxynucleotidyl transferase-mediated dUTP–fluorescein nick-end labeling.

DXR concentration change in the plasma after i.t. administration of the drugs. Blood was collected from a tail vein of mice at the indicated times after i.t. administration and the plasma samples were treated as described earlier. As shown in Table 2, doxorubicinon was detected 30 min after i.t. administration of PEG–DXR or PEG–DXR–oxSWNH. Their concentrations declined gradually for the following 2.5 h. After 24 h, they were not detected in either treatment. Importantly, the concentrations in the PEG–DXR–oxSWNH treatment at each time point were approximately 30% of those for PEG–DXR treatment. These results suggest that approximately 30% of PEG–DXR was released from PEG–DXR–oxSWNH as an initial burst and the rest (~70%) may be released relatively slowly below the detection limit of HPLC to reach 61% on day 21. Based on these HPLC analyses of doxorubicinon in the tumor homogenates on day 21 and the blood on day 7, the higher effectiveness up to day 13 in mice treated with PEG–DXR–oxSWNHs would be explained at least in part by the high DXR retention ability of oxSWNHs.

Histological analysis of the tumor tissues & adjacent lymph nodes of PEG–DXR–oxSWNH-treated mice

The photograph of a representative mouse administered i.t. with PEG–DXR–oxSWNH is shown in Figure 4A. A large part of the tumor surface was dyed black, indicating that PEG–DXR–oxSWNH could diffuse in the tumor tissue owing to its water-dispersibility. As described earlier, approximately 60% of DXR remained in the tumor 14 days after the initiation of i.t. administration of PEG–DXR–oxSWNHs (Table 2). From this observation, it is important to analyze the i.t. distribution of oxSWNHs histologically. The tumor tissues were excised on day 21 from mice i.t. treated with PEG–DXR–oxSWNH. Figure 4B shows their HE-stained sections. Black oxSWNH agglomerates were observed sparsely in the internal area (Figure 4B, middle) and densely in the peripheral area (Figure 4B, right) of the tumor. Vasculatures were observed in the area adjacent to oxSWNH agglomerates (Figure 4B, right), indicating no major inhibitory impact of oxSWNHs on tumor vascularization, while future investigation should address the detailed effects. Only a small amount of oxSWNH agglomerates were detected in liver and spleen (data not shown), suggesting the high retention ability of oxSWNHs themselves in the NCI-H460 tumor.

Water-dispersed charcoals accumulate in lymph nodes after local administration [27]. It is also reported that smaller water-dispersed charcoals migrate to lymph nodes more efficiently [28]. Because lymph nodes are one of the major sites of cancer metastases, the treatment of metastatic lymph nodes after detection is an important clinical challenge. Here, it was examined whether oxSWNH injected into the growing tumor tissue would migrate to the surrounding lymph nodes or not. Figure 4C shows axillary lymph nodes excised from mice on day 28 during the treatment schedule used in Figure 3. Clearly, the axillary lymph node of PEG–DXR–oxSWNH-treated mice was dyed black (Figure 4C, right). The staining was more apparent on day 36 (Figure 4D, right). OxSWNHs used in this study contain carbonaceous impurities, named giant graphitic ball, at 5%. Giant graphitic balls are over 10 times larger than oxSWNHs [24]. Consequently, these data suggest that i.t. administered PEG–DXR–oxSWNHs mainly migrate to and are retained in lymph nodes, similar to water-dispersed charcoals.

Interestingly, oxSWNHs were found to migrate selectively to the axillary lymph node among the inguinal, brachial and axillary lymph nodes (Figure 4D). Particularly, it should be noted that, among the three lymph nodes, the inguinal lymph node is closest to the tumor tissue in which PEG–DXR–oxSWNHs were injected. No microscopically detectable oxSWNH agglomerates were found in the histological sections either of the inguinal or brachial lymph nodes (data not shown). Black spots of oxSWNH agglomerates were found mainly in lymphatic sinuses, which are macrophage-rich regions of the axillary lymph node (Figure 4E, middle panel) [29]. They were also, to a lesser extent, detected directly beneath the surface region of the cortex (Figure 4E, right panel). The function of macrophages in lymphatic sinuses is to phagocytose particulate or persistent matter and soluble antigens flowing into lymph nodes [29]. These data indicate that the migration of oxSWNHs occurred through lymph ducts from the tumor tissue into the axillary lymph node. Based on the high DXR-retention ability of oxSWNHs (Table 2), oxSWNHs in the axillary lymph node may retain DXR derivatives, including PEG–DXR.

As shown in Figure 3, PEG–DXR–oxSWNHs showed a slightly higher *in vivo* antitumor activity than PEG–DXR did. To further confirm the effectiveness of PEG–DXR–oxSWNH, TUNEL staining of the tumor tissues isolated from mice on day 10 was performed. DNase I-treated tumor tissue as a positive control was stained strongly (Figure 5D), whereas the tissue from the untreated group was not (Figure 5A). Compared with the untreated tissue, it was clear that both tissues from PEG–DXR- and PEG–DXR-oxSWNH-treated mice were stained weakly but significantly (Figure 5B & 5C). This weak staining reportedly means that the cells are at an early stage of apoptosis prior to nuclear fragmentation and/or have single DNA-strand breaks that are repairable [30,31]. In fact, a similar two-grade staining in TUNEL was observed when cultured NCI-H460 cells were treated with PEG–DXR for 3 days (Figure 5F). Compared with the PEG–DXR-treated tumor section, the PEG–DXR–oxSWNH-treated one was clearly stained more broadly, suggesting that PEG–DXR–oxSWNH induced PEG–DXR-dependent DNA damage more than PEG–DXR did. This result would lead to superior *in vivo* antitumor activity of PEG–DXR–oxSWNH.